The Geological Society of America
Special Paper 550

Petrographic and chemical studies of the Cretaceous-Paleogene boundary sequence at El Guayal, Tabasco, Mexico: Implications for ejecta plume evolution from the Chicxulub impact crater

Tobias Salge
Natural History Museum, Imaging and Analysis Centre, Cromwell Road, SW7 5BD, London, UK; and
Museum für Naturkunde, Leibniz-Institut für Evolutions- und Biodiversitätsforschung, Invalidenstrasse 43, 10115 Berlin, Germany; and
Bruker Nano GmbH, Am Studio 2d, 12489 Berlin, Germany

Roald Tagle
Museum für Naturkunde, Leibniz-Institut für Evolutions- und Biodiversitätsforschung, Invalidenstrasse 43, 10115 Berlin, Germany, and
Bruker Nano GmbH, Am Studio 2d, 12489 Berlin, Germany

Ralf-Thomas Schmitt
Museum für Naturkunde, Leibniz-Institut für Evolutions- und Biodiversitätsforschung, Invalidenstrasse 43, 10115 Berlin, Germany

Lutz Hecht
Museum für Naturkunde, Leibniz-Institut für Evolutions- und Biodiversitätsforschung, Invalidenstrasse 43, 10115 Berlin, Germany, and
Institut für Geologische Wissenschaften, Freie Universität Berlin, Malteserstraße 74-100, 12249 Berlin, Germany

ABSTRACT

A combined petrographic and chemical study of ejecta particles from the Cretaceous-Paleogene boundary sequence of El Guayal, Tabasco, Mexico (520 km SW of Chicxulub crater), was carried out to assess their formation conditions and genetic relation during the impact process. The reaction of silicate ejecta particles with hot volatiles during atmospheric transport may have induced alteration processes, e.g., silicification and cementation, observed in the ejecta deposits. The various microstructures of calcite ejecta particles are interpreted to reflect different thermal histories at postshock conditions. Spherulitic calcite particles may represent carbonate melts that were quenched during ejection. A recrystallized microstructure may indicate short, intense thermal stress. Various aggregates document particle-particle interactions and intermixing of components from lower silicate and upper

Salge, T., Tagle, R., Schmitt, R.-T., and Hecht, L., 2021, Petrographic and chemical studies of the Cretaceous-Paleogene boundary sequence at El Guayal, Tabasco, Mexico: Implications for ejecta plume evolution from the Chicxulub impact crater, *in* Reimold, W.U., and Koeberl, C., eds., Large Meteorite Impacts and Planetary Evolution VI: Geological Society of America Special Paper 550, p. 207–233, https://doi.org/10.1130/2021.2550(08).

sedimentary target lithologies. Aggregates of recrystallized calcite with silicate melt indicate the consolidation of a hot suevitic component with sediments at ≥750 °C. Accretionary lapilli formed in a turbulent, steam-condensing environment at ~100 °C by aggregation of solid, ash-sized particles. Concentric zones with smaller grain sizes of accreted particles indicate a recurring exchange with a hotter environment.

Our results suggest that during partial ejecta plume collapse, hot silicate components were mixed with the fine fraction of local surface-derived sediments, the latter of which were displaced by the preceding ejecta curtain. These processes sustained a hot, gas-driven, lateral basal transport that was accompanied by a turbulent plume at a higher level. The exothermic back-reaction of CaO from decomposed carbonates and sulfates with CO_2 to form $CaCO_3$ may have been responsible for a prolonged release of thermal energy at a late stage of plume evolution.

INTRODUCTION

Large-scale impact cratering can interfere with the evolution of life on Earth, causing mass extinctions by introducing a massive amount of energy to the biosphere in a short time interval (Alvarez et al., 1980). It is widely accepted that the Chicxulub impact event on the Yucatán Peninsula caused the mass extinction observed at the Cretaceous-Paleogene boundary (ca. 65 Ma; e.g., Hildebrand et al., 1991; Swisher et al., 1992; Schulte et al., 2010; Renne et al., 2013; Hull et al., 2020). The Chicxulub impact structure has a diameter of ~180–200 km. It represents a peak-ring or multiple-peak-ring impact basin formed by a projectile with a diameter of ~10–14 km (e.g., Hildebrand et al., 1991; Swisher et al., 1992; Sharpton et al., 1993; Ivanov et al., 1996; Melosh, 2001; Stöffler et al., 2004; Morgan et al., 2016). The target rock at the impact site consists of an upper, ~3-km-thick sedimentary unit of the Yucatán platform, representing a carbonate-, sulfate-, and volatile-rich target sequence, and the underlying Pan-African silicate-rich crystalline basement (Lopez-Ramos, 1975; Krogh et al., 1993; Morgan et al., 1997). The release of climatically active gases that are associated with the vaporization of sulfates and carbonates may be relevant to environmental changes. SO_x gases, as well the emission of soot from impact-driven firestorms, may have caused a short, but probably severe cooling interval, whereas CO_2 gas may have led to subsequent long-term global warming (e.g., Kruge et al., 1994; Pierazzo et al., 1998; Harvey et al., 2008; Schulte et al., 2010; Brugger et al., 2017; Vellekoop et al., 2016; Artemieva et al., 2017; Tabor et al., 2020). The response of sedimentary target rocks to high shock pressures, however, is still not well understood (e.g., Langenhorst and Deutsch, 2012; Hamann et al., 2018; Salge et al., 2019; Hörz et al., 2020). For carbonates, vaporization (e.g., Kieffer and Simonds, 1980; Boslough et al., 1982; O'Keefe and Ahrens, 1989; Pierazzo and Artemieva, 2012; Hörz et al., 2015; Bell, 2016), melting (e.g., Graup, 1999; Osinski and Spray, 2001; Ivanov and Deutsch, 2002; Osinski et al., 2008; Walton et al., 2019), and calcite crystallization by the back-reaction of the decomposition products CaO and CO_2 (Agrinier et al., 2001; Yancey and Guillemette, 2008) are relevant processes that contribute to the total amount of CO_2 released to the atmosphere.

This article focuses on the marine Cretaceous-Paleogene boundary sequence of El Guayal in the state of Tabasco, Mexico, ~520 km southwest of the crater center (Fig. 1). A detailed petrographic and chemical study, with elemental mapping at high spatial resolution, was carried out to classify silicate and carbonate ejecta particles, and various aggregates such as accretionary lapilli. The goal was to provide insights into impact and alteration processes. Melting, aggregation, and thermal alteration processes during the initial stage of the Chicxulub impact

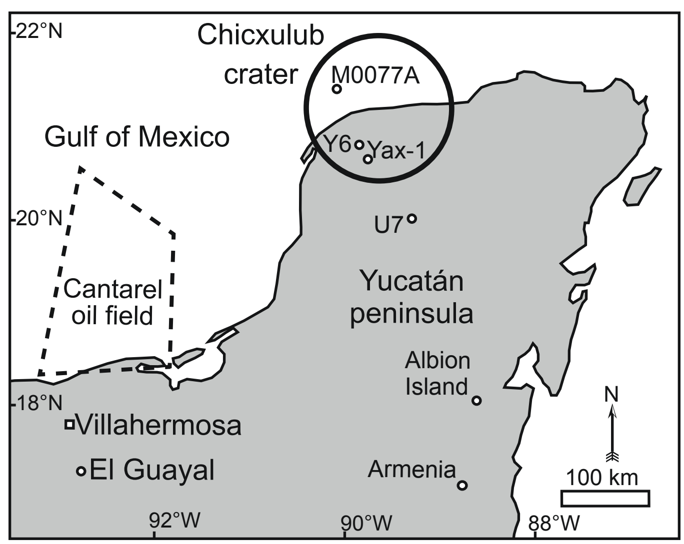

Figure 1. Map of the Yucatán Peninsula showing the outermost ring of the Chicxulub crater structure with drill sites: International Ocean Discovery Program (IODP)/International Continental Scientific Drilling Program (ICDP) Expedition 364 Hole M0077A, Yucatán-6 (Y6), ICDP Yaxcopoil-1 (Yax-1), UNAM-7 (U7), and the subaerially exposed proximal ejecta sites of Albion Island and Armenia, Belize, the Cretaceous-Paleogene site of El Guayal, Tabasco, Mexico, and the Cantarel oil field associated with the Cretaceous-Paleogene boundary (modified from Salge et al., 2019).

event and during prolonged ejecta transport will be discussed. The genetic relationships of impact products in the sedimentary record of El Guayal and data from proximal Cretaceous-Paleogene sections and suevites of the Chicxulub impact crater will help to improve ejecta plume evolution models. This study also aimed to elucidate the processes that contribute to the sealing properties of ejecta units, which is relevant for the offshore Cantarel oil fields located ~250 km north of El Guayal (Grajales-Nishimura et al., 2000, 2009).

STATE OF KNOWLEDGE

Cretaceous-Paleogene Boundary Sequence of El Guayal, Mexico

The riverbanks of El Guayal (17°32′37.73″N, 92°36′07.61″W) in the state of Tabasco, Mexico, expose a complete Cretaceous-Paleogene section of ~100 m thickness (Sigurdsson et al., 1995; Griscom et al., 1999, 2003; Grajales-Nishimura et al., 2000, 2009; Arenillas et al., 2006; Dubron et al., 2006; Schulte et al., 2010). Paleogeographic reconstructions for the Late Cretaceous show that this area represented the shelf region of the Yucatán Peninsula at water depths of several hundreds of meters (Smit, 1999). A complex clastic unit was deposited between two pelagic formations, the underlying Jolpabuchil Formation (Campanian–Maastrichtian) and the overlying Soyaló Formation (Paleocene) (Arenillas et al., 2006). The complex clastic unit is a fining-upward succession that can be divided into four subunits from the top to the base (Fig. 2). The lowest subunit 1 is an ~40-m-thick monomict, coarse carbonate megabreccia. It contains large limestone blocks up to 2 m in size at the base and grades into a fine-grained, carbonate breccia at the top. Subunit 2 is ~5 m thick, is clearly graded, and transits upward into a coarse-grained calcareous sandstone. The polymict carbonate microbreccia contains rare impact ejecta such as quartz with microdeformation features and altered silicate melt particles. Subunit 3 is rich in impact ejecta and ~6 m thick, grading from coarse calcareous sandstone to fine-grained, thin-bedded, cross-bedded sandstone near the top. At the base of subunit 3, there occur accretionary lapilli. The average dimensions determined from a set of 24 accretionary lapilli are 1.3 × 1.1 × 0.8 cm, with an average aspect ratio of 0.59 (Burns et al., 2003). The accretionary lapilli consist of ash-sized particles such as clay-altered silicate melt fragments, calcite, dolomite, and quartz in a microcrystalline, authigenic SiO_2 matrix (Griscom et al., 1999; Grajales-Nishimura et al., 2009). Electron-spin-resonance studies show an SO_3^--enhanced signature for calcite in the accretionary lapilli that indicates formation in the ejecta plume, either from condensation in the presence of CO_2/SO_3-rich vapors, or by reactions between solid CaO and CO_2/SO_3-rich vapors (Griscom et al., 1999, 2003). The uppermost layer, subunit 4, is a thin, 1-cm-thick, yellow to red clay layer where an impactor component has been identified by elevated platinum group elements (PGEs; Goderis et al., 2013). On top of the complex clastic unit, the lowermost Danian *Hedbergella holmdelensis* subzone (= biozone P0) was identified in a 3–4-cm-thick dark clay bed (Arenillas et al., 2006). The sedimentologic, mineralogical, and stratigraphic evidence indicates that the complex clastic unit was formed during the impact event: (1) Seismic activity caused by the shock wave of the impact resulted in fracturing and collapse of the slopes of the Yucatán platform and deposition of a monomict carbonate megabreccia in sedimentary gravity flows at El Guayal near the shelf region of the Yucatán platform, and this was followed by the (2) arrival of ballistically emplaced impact ejecta from the Chicxulub crater; (3) reworking and deposition, possibly induced by tsunami currents; and (4) deposition of globally distributed ejecta with a small proportion of the projectile component.

The stratigraphic succession of El Guayal can be correlated to the offshore Cantarel oil fields, ~250 km north of El Guayal (Fig. 1). At the western Campeche platform, an ~300-m-thick dolomitic carbonate megabreccia is the oil-producing reservoir facies, and the overlying ~30-m-thick reworked ejecta and breccia lenses represent the sealing facies (Grajales-Nishimura et al., 2000, 2009). Those oil-producing units at the western Campeche marine platform are considered to be the most important oil field related to an impact event.

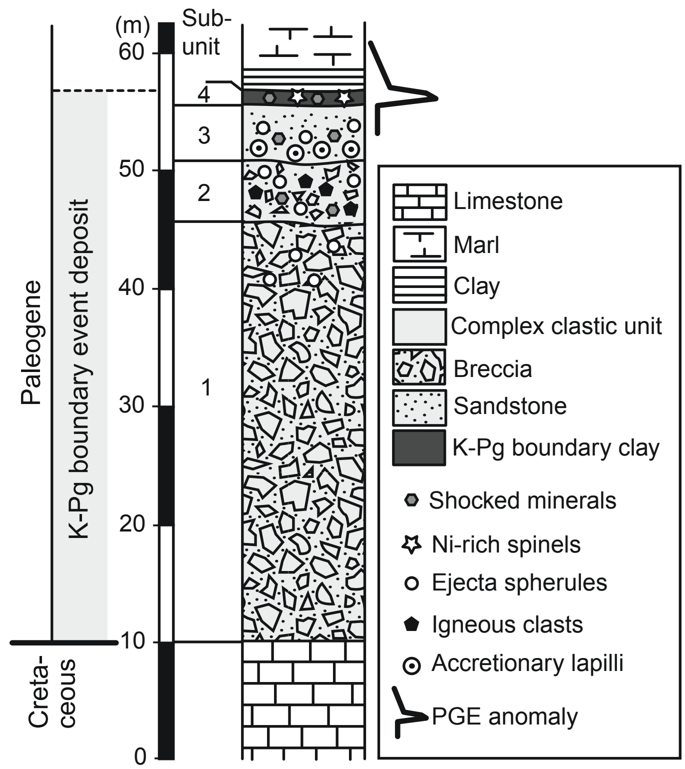

Figure 2. Schematic stratigraphic column of the Cretaceous-Paleogene (K-Pg) boundary sequence at El Guayal, Tabasco, Mexico (modified from Schulte et al., 2010). The Cretaceous-Paleogene boundary clay (subunit 4) is 1 cm thick and not to scale. PGE—platinum group element.

Characteristics of Proximal to Distal Chicxulub Ejecta Deposits

The Chicxulub impact event deposited an ejecta layer that decreases in thickness with distance from the impact crater. At the UNAM-7 borehole near the outer crater rim (Fig. 1), a >400-m-thick impact-breccia sequence was deposited (Urrutia-Fucugauchi et al., 1996, 2014; Salge et al., 2019). Here, a polymict suevitic breccia that is rich in altered silicate melt particles from crystalline target lithologies overlies an evaporite-rich megabreccia. On the southern Yucatán Peninsula, the Chicxulub ejecta blanket has been identified at sites 280–470 km from the crater center (Ocampo et al., 1996; Pope et al., 1999, 2005; Fouke et al., 2002; King and Petruny, 2003, 2015; Kenkmann and Schönian, 2006; Kletetschka et al., 2020). These ejecta deposits are represented as a 2–5-m-thick lower spheroid bed, composed of silicate melt particles, accretionary lapilli, and pebble-sized clasts in a fine-grained matrix, which extends up to Armenia, Belize (Fig. 1), 470 km from Chicxulub. The overlying diamictite is up to 15 m thick, composed of carbonate clasts up to 9 m in size, silicate melt particles, and rare shocked quartz grains, and it extends up to 360 km distance at the site of Albion Island, Belize (Fig. 1). In the Gulf of Mexico and the Caribbean Sea, a mixture of microfossils, impact ejecta particles, and lithic fragments was deposited by sedimentary gravity flows (e.g., Alvarez et al., 1992; Bralower et al., 1998; Arenillas et al., 2006; Grajales-Nishimura et al., 2009). At more proximal distances of 500–1000 km from Chicxulub, around the northwestern Gulf of Mexico, the marine Cretaceous-Paleogene boundary sites are represented as centimeter- to meter-thick ejecta-rich, clastic deposits indicating high-energy transport by tsunami waves (e.g., Smit et al., 1996; Schulte et al., 2012). At intermediate distances of 1000–5000 km from Chicxulub, a dual-layer stratigraphy can be observed at marine and terrestrial Cretaceous-Paleogene boundary sites (e.g., Bohor et al., 1987; Izett, 1990; Norris et al., 1999; MacLeod et al., 2007; Schulte et al., 2009, 2010). A 2–10-cm-thick ejecta layer is composed of altered silicate melt particles and overlain by a 0.2–0.5-cm-thick layer. The upper layer is enriched in shocked minerals, Ni-rich spinels, and an impactor component as evidenced by the enrichment of PGEs. In distal marine sections more than 5000 km from Chicxulub, the ejecta layer at the Cretaceous-Paleogene boundary is represented by red clay with a thickness of 2–5 mm and a local maximum of 3 cm (e.g., Montanari et al., 1983; Montanari, 1991; Smit, 1999; Schulte et al., 2010).

Emplacement Models for Chicxulub Ejecta Deposits

The process of impact cratering is reasonably well understood (e.g., Melosh, 1989; French, 1998). Target material is ejected ballistically in a laterally expanding ejecta curtain. A turbulent, hot ejecta plume with vaporized projectile material is lifted to the stratosphere. The dual-layer stratigraphy at intermediate Cretaceous-Paleogene boundary sites has been explained by (1) much faster arrival of ballistic ejecta that were emplaced in the ejecta curtain forming the majority of the ejecta deposit, and (2) longer deposition time of material that was transported in the turbulent ejecta plume forming the global fireball layer (e.g., Smit et al., 1992; Pollastro and Bohor, 1993; Smit, 1999; Kring and Durda, 2002; Schulte et al., 2009). A more complex ejecta emplacement is indicated by the presence of accretionary lapilli and accretionary calcite clasts at proximal to intermediate Cretaceous-Paleogene sites (e.g., Alegret et al., 2005; Pope et al., 2005; Schulte and Kontny, 2005; Schulte et al., 2006, 2009, 2010, 2012; Yancey and Guillemette, 2008). Studies of the impact ejecta blanket at Stac Fada, Scotland, have shown that the accretionary lapilli–bearing suevite was emplaced as stratified density currents that are comparable to volcanic pyroclastic density currents. Other models have been suggested that address the physical differences of impact events that eject material with much lower density and an order of magnitude higher initial velocity compared to volcanic events: (1) Johnson and Melosh (2014) have shown that accretionary lapilli can form within the ejecta curtain early in the ejection process, well before reentry into the atmosphere or ballistic emplacement. (2) Huber and Koeberl (2017) suggested a mechanism for upper atmospheric accretion: A dense cloud of ash forms during reentry from the stratosphere to the atmosphere at altitudes of neutral buoyancy; upon collapse, distal pyroclastic-like deposits and accretionary lapilli with an impactor component can form. (3) The melt fuel-coolant interaction (MFCI) of an impact melt sheet with water results in explosive phreatomagmatic activity and fragmentation of impact melt (Grieve et al., 2010; Stöffler et al., 2013; Artemieva et al., 2013; Osinski et al., 2019).

The unusual Chicxulub target lithologies may have had a strong influence on the ejecta emplacement. Belza et al. (2017) have shown that the heterogeneous, layered, and volatile-rich target contributed significantly to the formation of a dust-rich environment, and the preservation of some degree of heterogeneity in the ejecta plume. Alvarez et al. (1995) and Pope et al. (1997) proposed the formation of an ejecta plume doublet in the earliest stage of the impact event. The inner, hot plume consisted of vaporized target rock and meteorite components. The outer, warm plume was less energetic and dominated by vaporized and condensed sedimentary target material and steam with little projectile contribution. Sharpton et al. (1999) noted that the high content of primary ejecta at borehole UNAM-7, and the preservation of ejecta as 60-m-thick evaporite megaclasts in a fine-grained, weakly shocked, carbonate-anhydrite–rich matrix are in contrast with ejecta characteristics predicted by purely ballistic sedimentation. They discussed that these features indicate that these deposits were possibly emplaced as flow deposits as strongly "heated masses of gas-charged debris" transported more or less horizontally (Sharpton et al., 1999). Pope et al. (2005) suggested that steam explosions from instantly vaporized target water led to flow-like transport processes: An initial flow involved a volatile-rich cloud of fine debris similar to a volcanic pyroclastic flow forming the spheroid bed on the southern Yucatán Peninsula. A later flow of coarse debris may not have extended much beyond

3.6 crater radii, forming the diamictite bed at Albion Island by the turbulent collapse of the ejecta curtain. Kenkmann and Schönian (2006), furthermore, showed that the ejecta blanket on the southern Yucatán Peninsula was emplaced as a ground-hugging, erosive, and cohesive secondary ejecta flow, and that the large runout was related to subsurface volatiles.

Sedimentary Ejecta Particles of the Chicxulub Impact Event

The identification of sedimentary ejecta remains complex; e.g., the identification of carbonate melts, and their discrimination from physical-chemical-precipitated carbonates or biogenic carbonates, is challenging because carbonate melts do not quench to glasses. Chicxulub impactites and Cretaceous-Paleogene ejecta deposits, however, reveal that sedimentary ejecta display great variability, indicating various degrees of shock metamorphism, followed in part by thermal overprinting during ejection and atmospheric transport. Salge et al. (2019) described impact-induced recrystallization and decomposition for anhydrite clasts at the UNAM-7 drill core. The lack of anhydrite in the crater suevites from the drill cores Yaxcopoil-1 (e.g., Dressler et al., 2004; Kring et al., 2004) and International Ocean Discovery Program (IODP)/International Continental Scientific Drilling Program (ICDP) Expedition 364 Hole M0077A (Gulick et al., 2017a), as well as in the Cretaceous-Paleogene ejecta deposits, may indicate that sulfates were completely dissociated at high temperature (T > 1465 °C), whereas ejecta deposited close to the outer crater rim experienced postshock conditions that were less effective at dissociation (Salge et al., 2019). "Feathery"-textured calcite particles from the evaporite-rich megabreccia of the UNAM-7 borehole (Salge et al., 2019) were also described at the upper part of the suevite of the Yucatán-6 borehole in the Chicxulub impact crater (Jones et al., 2000; Claeys et al., 2003). The "feathery" texture seems to resemble the radiating, spherulitic microstructure indicative of quenching of carbonate melts at high cooling rates, i.e., several hundreds of degrees Celsius per second (Fig. 3; Jones et al., 2000).

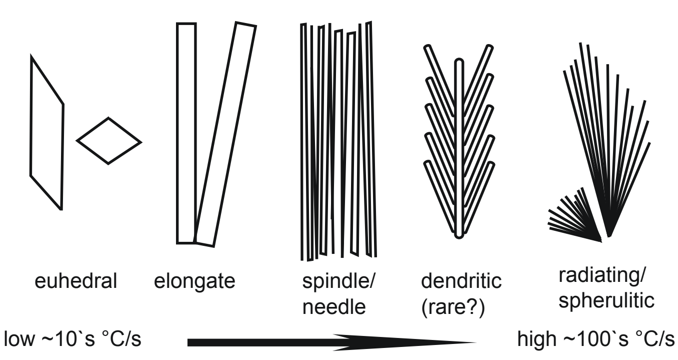

Figure 3. Carbonate melt microstructures as a function of cooling rate/degree of undercooling (modified from Jones et al., 2000).

Ejecta at proximal to intermediate Cretaceous-Paleogene sites are commonly composed of silicate melt particles that are associated with calcite: Quenched carbonate melts are indicated in calcite inclusions by "needle," feathery," and "cauliflower" textures and an equilibrium texture with 120° triple junctions (Schulte et al., 2003, 2012; Schulte and Kontny, 2005). Welding, fusing, and amalgamation with emulsion-like textures between silicic and carbonate phases, as well as the enveloping of marl and benthic foraminifera by altered silicate melt, suggest the interaction of hot silicic ejecta with marine sediments on the northeastern Mexican shelf (Schulte and Kontny, 2005). A different formation process is indicated by accretionary calcite clasts 50 µm to 3 mm in diameter at Cretaceous-Paleogene sections around the Gulf of Mexico, North America, and in the borehole from Ocean Drilling Program (ODP) Site 207 (e.g., Schulte et al., 2006, 2009, 2010, 2012; Yancey and Guillemette, 2008). They consist of micrometer-sized calcite subgrains that are associated with altered silicate melt and porosity. They have been interpreted to represent accretionary lapilli that originated from calcite crystals generated within the Chicxulub ejecta plume from back-reaction of decomposition products (Yancey and Guillemette, 2008).

ANALYTICAL METHODS

Between 1998 and 1999, 42 samples were collected by Philippe Claeys during field trips to El Guayal. In total, 31 thin sections were taken of bulk rock samples from the complex clastic unit (two of the uppermost subunit 1, 13 of subunit 2, 15 of subunit 3, one of subunit 4); eight accretionary lapilli and six particles from the lower subunit 3 were also analyzed.

Light and Scanning Electron Microscopy

Immersion oil was used for micrographs acquired with 50× and 100× objectives for optimal resolution. Mosaic binocular micrographs of 14 thin sections were taken with crossed polarizers. Scanning electron microscopy (SEM) was carried out using a JEOL JSM-6300 instrument at the Museum für Naturkunde, Berlin (MfN), equipped with a Röntec energy dispersive spectrometry (EDS) system and Si(Li) detector. To enable navigation and assist in the choice of areas to be analyzed, mosaic backscattered-electron (BSE) micrographs of two accretionary lapilli were prepared. A high-resolution elemental map (3048 × 4096 pixels, 410 nm pixel size) of the lapilli-bearing rock was acquired using a ZEISS Supra 55 field emission SEM at Bruker Nano GmbH, Berlin, equipped with a Bruker Quantax EDS system and XFlash silicon drift detector. To enhance the spatial resolution for element analysis, an intermediate acceleration voltage of 10 kV was applied.

Electron Microprobe Analyses

Quantitative analysis of silicate melt particles was performed using a JEOL JXA-8800 electron microprobe (EMP) at MfN. The analyses were performed point by point (manual mode), to allow better control of the measured position. Analyses were calibrated using reference samples for electron microprobe analyses from the U.S. National Museum (Jarosewich et al., 1980, 1987) and Astimex Scientific Limited, MINM25–53 (see Supplemental Material[1]). An acceleration voltage of 15 kV, a beam current of 15 nA, and an electron beam diameter of 3 µm were used; for small grains, beam sizes of 1 µm were used. Acquisition time was 20 s for the peak and 10 s for the background. To minimize loss of the volatile elements, Na and K were analyzed first. Detection limits for all elements were determined from a large number of reference analyses (see Supplemental Material): 105 for basaltic glass, 101 for tektite glass, 49 for microcline, 53 for plagioclase, and 31 for anorthoclase. In order to control the stability of the calibration, certified reference samples were measured after each 10 measurements.

Cathodoluminescence Studies

Cathodoluminescence (CL) microscopy was carried out to discriminate different carbonate generations. The intensity is dependent on the counterbalance of activators such as Mn^{2+}, or rare earth elements and quenchers like $Fe^{2+/3+}$, Ni^{2+}, and Co^{2+}. Mn^{2+}-activated luminescence has a yellow to orange/red color (Machel et al., 1991). If the total Fe is <150 µg/g, low levels of Mn^{2+} (10–20 µg/g) can produce a detectable luminescence (Machel et al., 1991; Neuser et al., 1996). A hot cathodoluminoscope Lumic HC3-LM system at MfN was operated at 14 kV and 0.08–0.25 mA. A Kappa Image Base DX 20 HC thermoelectronically cooled camera was used to obtain low-intensity CL images.

Chemical Analyses

For bulk-rock analyses, samples were ground using a steel mortar. For a second batch, a corundum mortar was used to exclude contamination by metal during grinding. Major and trace elements were determined by X-ray fluorescence spectroscopy (XRF) with a Siemens SRS-3000 at MfN on glass tablets. Details of sample preparation, applied international certified rock standards, detection limits, and analytical errors were given by Schmitt et al. (2004). For loss on ignition (LOI), ~1 g of pulverized sample material, dried for 4 h at 105 °C, was used. The sample material was heated in porcelain crucibles for 4 h at 1000 °C. The LOI was calculated using the weight difference from before and after heating. Detection limit, precision, and accuracy values for LOI were ~0.1 wt%. The CO_2 concentration of the samples was measured by infrared spectroscopy with a Rosemount CWA 5003 analyzer at MfN. Depending on the LOI, between 0.2 and 2 g aliquots of pulverized sample material, which was dried for 4 h at 105 °C, were used for the analyses. The temperature for the thermal decomposition and/or oxidation of the sample to release CO_2 was set to 990 °C, and synthetic $CaCO_3$ pro analysis (≥99 wt%) was used as reference material. The detection limit of this method was 0.1 wt% CO_2, and the precision and accuracy values for were also ~0.1 wt% CO_2.

PGE concentrations were measured at the GeoForschungsZentrum, Potsdam, Germany, using an inductively coupled plasma–mass spectrometer following nickel sulfide fire assay preconcentration and separation steps (Tagle et al., 2004; Goderis et al., 2013).

Modal Composition Calculations

XRF bulk-rock and EMP phase compositions were used to calculate the proportion of each phase under investigation. The calculation of the modal composition for each of the 12 samples was performed using the computer program PETMIX (http://www.geologynet.com/programs/petmix410.xls), which is based on the constrained mixing model of Le Maitre (1979) and the method of least squares (Davis, 1973). For the lower subunit 3, where individual accretionary lapilli are common, individual calculations for both accretionary lapilli and the host rock were performed.

RESULTS

Stratigraphy, Lithology, and Petrography of El Guayal Units

Subunit 1

The monomict carbonate megabreccia contains angular to subrounded carbonate fragments in a matrix of carbonate mud with isolated foraminifera and shell fragments. The following carbonate microfacies were identified with a binocular: foraminifera grainstone; intraclastic foraminifera-bearing wackestone; fine detritic packstone; packstone to grainstone with foraminifera, ostracodes, and gastropods; biogenous packstone to grainstone to rudstone with foraminifera, corals, shell fragments, and bryozoan clasts; slight laminated mudstone; mudstone to wackestone with small components; foraminifera-bearing wackestone; and biogenic clasts like Cretaceous rudist bivalves (*Hippurites*, Radiolitidae). The overlying fining-upward, ~3.5-m-thick unit shows a reduction in clast size to 0.5–2 cm. Calcite clasts are common, dolomite clasts are present, silicates are very rare, and silicification of calcite was not observed.

Subunit 2

The megabreccia grades into an ~5-m-thick polymict carbonate microbreccia containing silicate ejecta particles (Figs. 4A and 4C). The clastic unit fines upward with clast sizes from <5 mm (rarely 2 cm) at the base to <2 mm (rarely 5 mm) at the top. Silicate melt particles that had altered to clay minerals are

[1]Supplemental Material. Transmitted light and back-scattered electron (BSE) micrographs of silicate melt-coated calcite aggregates and silicate melt particles, high-resolution energy-dispersive spectrometry elemental map, high-resolution BSE mosaic of accretionary lapillus, X-ray fluorescence analyses of bulk rock and accretionary lapilli, electron microprobe analyses of silicate melt particles, and modal composition calculations. Please visit https://doi.org/10.1130/SPE.S.14736894 to access the supplemental material, and contact editing@geosociety.org with any questions.

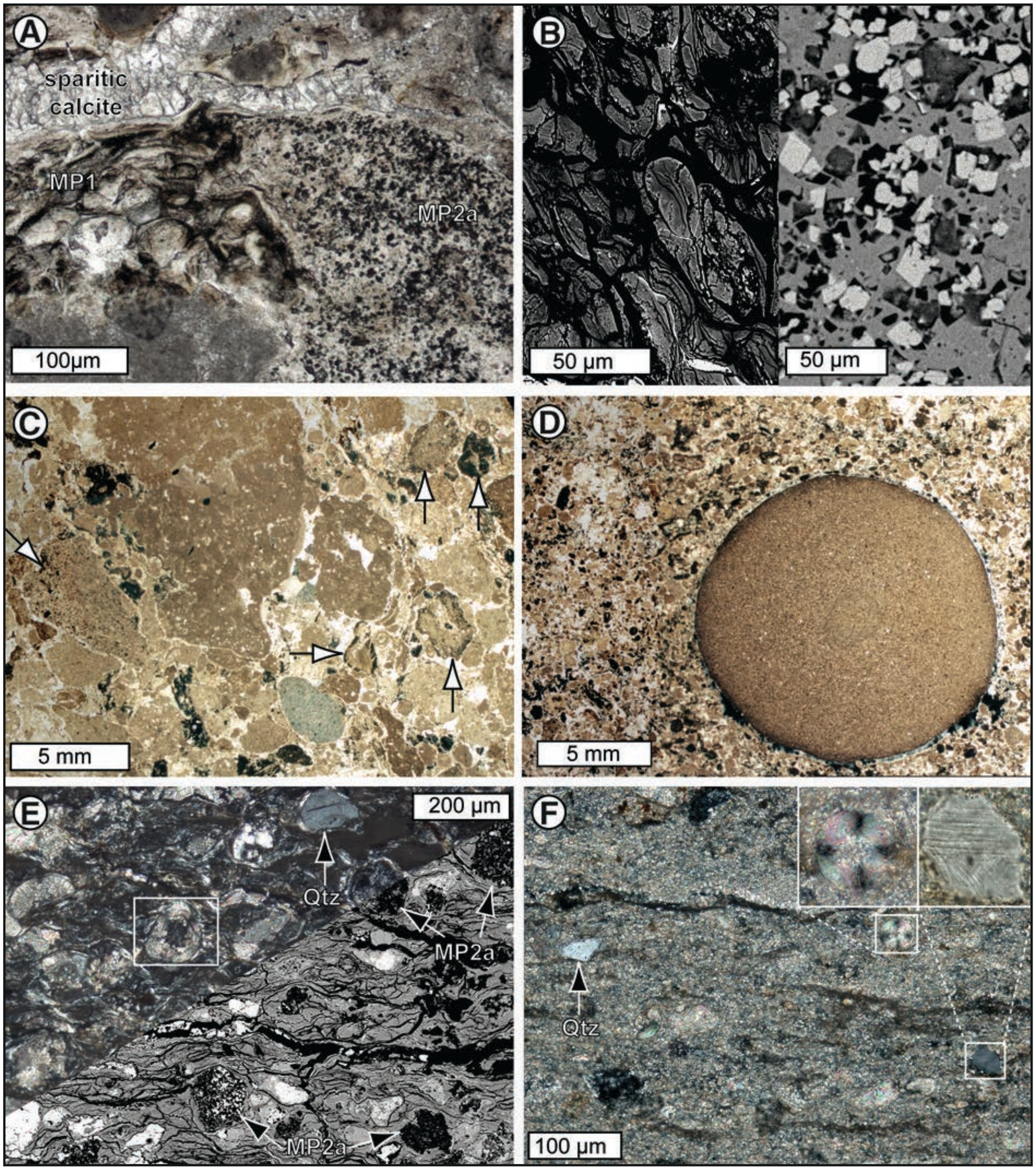

Figure 4. Melt particles types in the ejecta units and unit overview of the Cretaceous-Paleogene site of El Guayal, Tabasco, Mexico. (A) Micrograph (plane-polarized light, PPL) from lower subunit 2 showing melt particle type 1 (MP1) and melt particle type 2a (MP2a). (B) Backscattered-electron (BSE) micrographs from lower subunit 2 showing MP1 (left) with a distinct flow texture and MP2a (right) with microcrystalline calcite (bright) and pseudomorph pore space (dark). (C) Binocular mosaic micrograph (cross-polarized light, XPL) from subunit 2 showing altered silicate melt particles (dark) and micritic calcite clasts (brown). Sparitic calcite (bright) is present between clasts. Arrows—aggregates consisting of calcite with rims of altered silicate melt. (D) Binocular mosaic micrograph (XPL) from lower subunit 3 with accretionary lapillus. (E) Micrographs (XPL, BSE) of the uppermost, cross-bedded subunit 3 where clay minerals are the major component of the matrix. Calcite particles have spherulitic to recrystallized microstructures (left). Rectangle shows a spheroidal calcite aggregate with silicate melt nucleus (see Fig. 10A). On the right side, calcite particles are almost absent, and MP2a does not contain any microcrystalline calcite, only pseudomorph pore space. Qtz—quartz grain. (F) Micrograph (XPL) of subunit 4 showing a marly matrix with a quartz (Qtz) grain. Magnifications shows a spherulitic calcite spheroid (left, XPL) and a shocked quartz particle (right, PPL) with multiple sets of planar deformation features.

observed in hand specimens as greenish particles. Microscopic studies revealed a well-preserved morphology of the silicate melt particles. Vesicular fragments with thin walls are rare. Two major types of altered silicate melt particles were distinguished according to the absence (melt particle type 1, MP1) or presence (melt particle type 2a, MP2a) of various degrees of microcrystalline calcite, associated with small-sized porosity (Figs. 4A and 4B, respectively). MP1 appears as subrounded to angular bodies, often with vesicular morphology and a characteristic flow texture. MP2a is represented as aggregates composed of microcrystalline calcite with silicate melt; MP2a rarely contains degraded microfossils (Supplemental Fig. S1). MP2a has a typical pore space between <1 µm and 30 µm in diameter, which often displays a pseudomorph, hexagonal shape that resembles former calcite crystals. The ratio of silicate melt, calcite, and pore space for MP2a varies for different particles.

Quartz and feldspar grains with shock metamorphic features including planar deformation features (PDFs, commonly decorated) and undulatory extinction are present in subunit 2. Some carbonate ejecta particles consist of pure calcite with spherulitic microstructures. Other calcite particles display a microstructure of unoriented, fine-grained crystals with locally larger crystal

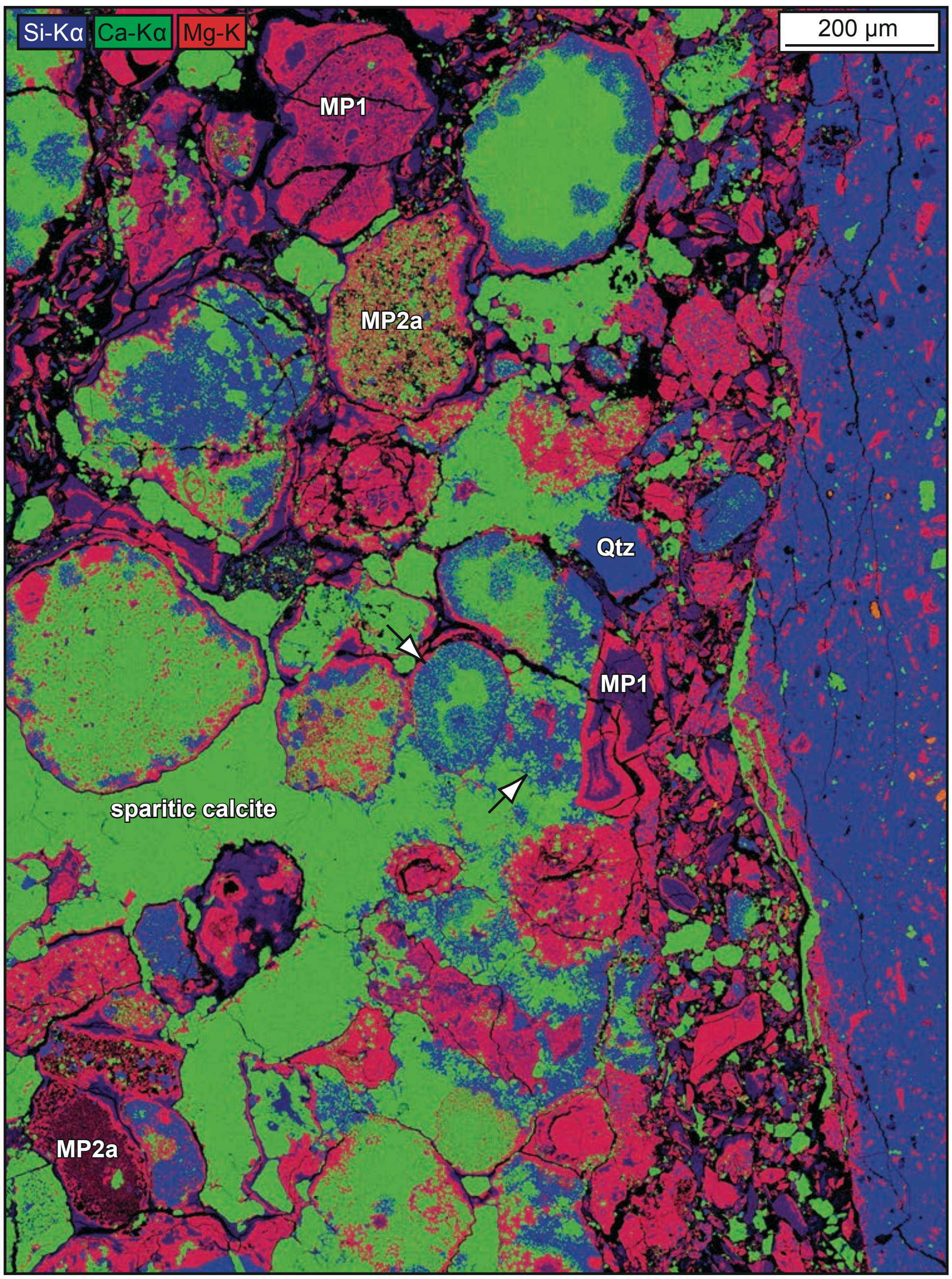

Figure 5. High-resolution energy dispersive spectrometry (EDS) composite elemental map (10 kV, 3048 × 4096 pixel, 410 nm pixel size) of lower subunit 3 showing a polymict, carbonate ejecta breccia and the outer rim of an accretionary lapillus (right). SiO_2 is represented by a blue color for silicon; calcite is represented by a green color for calcium. A loss of SiO_2 in heterogeneous altered silicate melt particles (melt particle type 1 [MP1], purple—high SiO_2, low MgO; pink—low SiO_2, high MgO) is associated with silicification (arrows) predominantly at the rim of calcite clasts and less pronounced at sparitic calcite in the interconnected pore space. Clasts of melt particle type 2a (MP2a) contain varying amounts of silicate melt, recrystallized calcite, and pore space (see also Supplemental Fig. S4 [see text footnote 1]). Qtz—quartz.

sizes that are indicative of recrystallization; this microstructure will be described as recrystallized. The pore space of the clast-supported breccia and vesicles of silicate melt particles are filled with secondarily precipitated, coarse-grained sparitic calcite (Fig. 4A). Silicification can be observed in fine-grained calcite particles, beginning from the outer grain boundaries. In the void-filling sparitic calcite, silicification is less pronounced.

Subunit 3

The 6-m-thick subunit 3 can be readily distinguished from the underlying subunit 2 by its yellowish color. This coloration is caused by increased staining of iron hydroxides/oxides due to the pronounced alteration of impact melt, and it can be observed as rust-like areas in hand specimens. In subunit 3, there are more altered silicate melt particles and calcite particles with spherulitic to recrystallized microstructures than in subunit 2. The aggregation of silicate melts with calcite, and the silicification of calcite are also more pronounced in subunit 3.

The lower subunit 3 is less well sorted than the underlying subunit 2. Carbonate clasts >5 cm and silicate melt particles >2 cm are observed, although the majority of the clasts and particles are <2 mm in size. Accretionary lapilli are abundant in the lower subunit 3 and well preserved (Figs. 4D and 5). Similarly sized aggregates are present as zoned, subrounded particles with a core of recrystallized calcite and a rim of altered silicate melt (Supplemental Fig. S2). The middle subunit 3 is well sorted, with particle sizes of <2 mm, and it is poor in accretionary lapilli. The laminated silt beds in the upper subunit 3 consist of a matrix of clay minerals. Within this matrix, embedded recrystallized calcite particles and silicate melt particles (MP2a) are <150 µm in size (Fig. 4E, left side). At the uppermost subunit 3, near the contact with subunit 4, a distinct boundary is observed; this boundary is caused by an abrupt lack of calcite particles (Fig. 4E, right side). Additionally, MP2a does not contain any microcrystalline calcite, only pseudomorph pore space.

Subunit 4

The transition of subunit 3 toward subunit 4 is marked by a sudden change in the main matrix component; microscopic studies documented this change from clay minerals to a fine-grained, marly matrix (Fig. 4F). This unit contains spherulitic calcite spheroids and fragments. Compared to the underlying units, more quartz particles were observed; these often showed multiple sets of well-preserved PDFs (Fig. 4F).

Chemistry of Bulk Rock and Melt Particles with Modal Content Calculations

Bulk Rock and Accretionary Lapilli

The major- and trace-element concentrations of El Guayal bulk rocks (see Supplemental Table S1) reflect the petrographic observations of two-component mixing of silicate and carbonate components. Harker diagrams for the plotted mean bulk-rock compositions versus SiO_2 (Fig. 6) show a negative correlation with SiO_2 for CaO and Sr, with the highest values in the monomict carbonate megabreccia (subunit 1). A positive correlation is present for K_2O, with highest values found in subunit 4. The accretionary lapilli and their host rock show comparable trace-element concentrations for Ba, Cr, V, Ti, and Zr. Analyses of PGEs were performed for the accretionary lapilli and their surrounding host rock (bulk rock of lowermost subunit 3 without accretionary lapilli; Table 1). Figure 7 shows the carbonaceous chondrite (CI)–normalized PGE abundances for the accretionary lapilli and their host rock; neither the accretionary lapilli nor the host rocks are enriched in PGEs. Compared to the overlying subunit 4, where PGE concentrations are an order of magnitude higher than in the continental crust (Goderis et al., 2013), in the lowermost subunit 3, no impactor component was identified in the accretionary lapilli and the host rock.

Heterogeneous Altered Silicate Melt Particles

The altered silicate melt particles of the bulk rock and accretionary lapilli are heterogeneously composed. Light microscopic studies with plane-polarized light displayed brownish stained areas of iron hydroxides/oxides. SEM-EDS and EMP studies revealed variation between two compositions (Table 2; Fig. 5). The average composition of the altered melt particles clearly indicates that high FeO and MgO values correspond to a decrease in SiO_2, K_2O, Al_2O_3, CaO, and Na_2O. The loss of SiO_2 in altered silicate melt particles and its association with the replacement of calcite by silica (Fig. 5) indicate postdepositional silica release and cementation.

Modal Content

The calculated modal content confirms the observation of a two-component mixing trend between a carbonate endmember and a clay-altered silicate melt endmember. Significant changes in mineralogical composition are correlated with lithological contacts (Table 3). The modal content is in good agreement with the petrographic observations, specifically (1) a decreasing modal content of calcite and increasing modal content of clay minerals, predominantly from altered silicate melt, from the base to the top of the sequence; (2) an absence of dolomite in the middle and upper subunits 2 and 3; and (3) a substantial increase in SiO_2, from quartz grains, in subunit 4.

Description of Ejecta and Their Aggregates

Accretionary Lapilli

The internal texture of the accretionary lapilli and the shapes of accreted particles are well preserved. Broken hand specimens show several continuous concentric zones ~1 mm in size (Fig. 8A). The ash-sized particles are dispersed in a matrix of silica. Remnant areas of microcrystalline calcite show a similar silicification texture as seen for fine-grained calcite particles of the bulk rock, which suggests a former calcite matrix that has been replaced by silica.

Most of the accreted particles have grain sizes between 10 and 100 µm. The maximum grain size is ~150 µm, with occasional

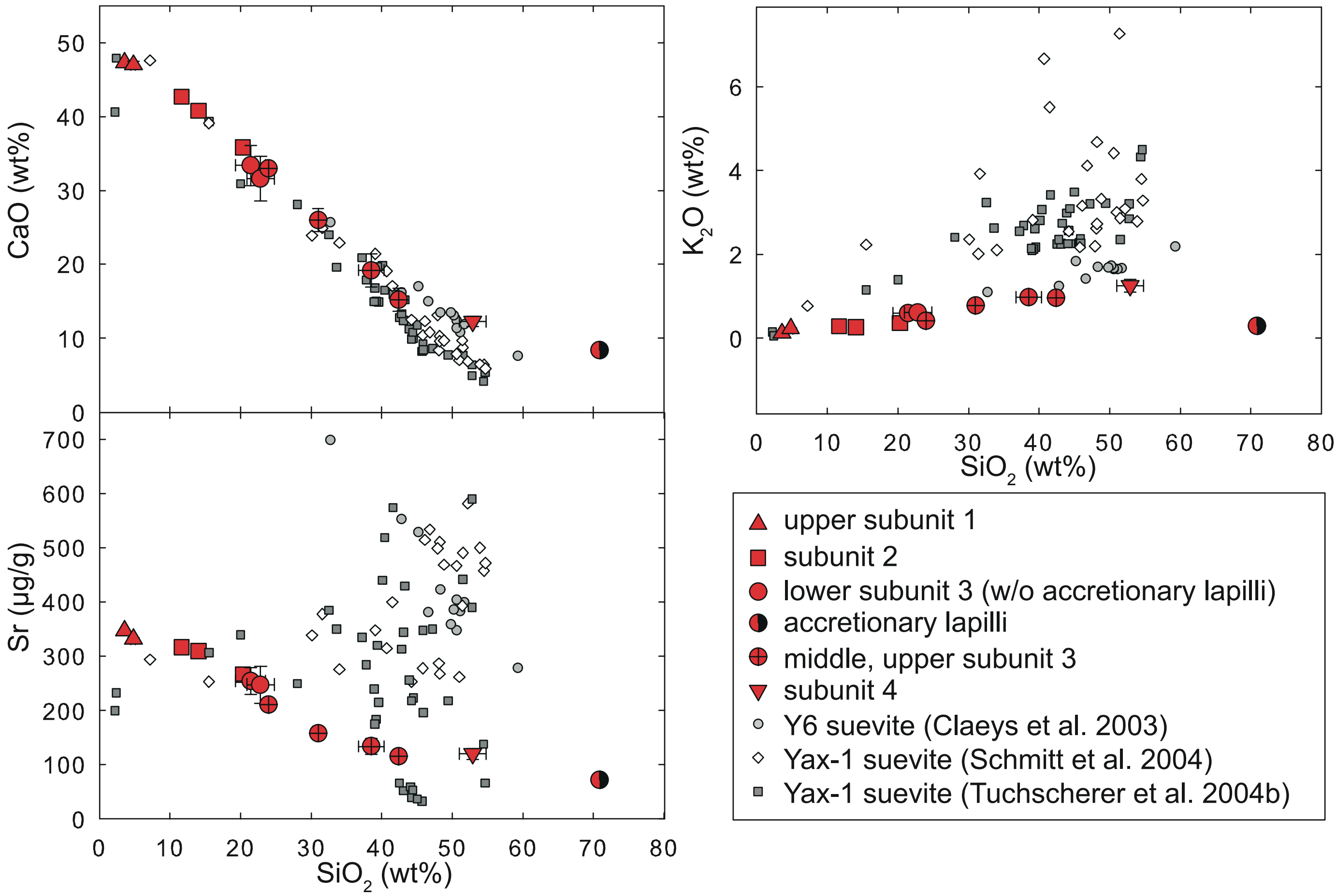

Figure 6. Harker diagrams of mean X-ray fluorescence (XRF) values for selected elements of El Guayal bulk rock and accretionary lapilli compared with Y6 suevite (Claeys et al., 2003) and Yax-1 suevite (Schmitt et al., 2004; Tuchscherer et al., 2004b) of the Chicxulub impact structure. For a better view, Yax-1–852.80 (Schmitt et al., 2004) has been excluded due to unusually high Sr concentration.

larger particles >300 µm. Within the core, the particles are more randomly distributed than toward the edges, where elongate particles are aligned tangentially to the lapilli rim (Fig. 8B; Supplemental Fig. S5). The concentric zones correspond to a decrease in the size of accreted particles, which also can be observed both near the rim of the accretionary lapilli and around vesiculated, altered silicate melt nuclei >1 mm in diameter.

Modal composition calculations indicate a content of 19 vol% clay minerals from altered silicate melt, 11 vol% calcite, and 6 vol% dolomite (Table 3). The diagenetic silica matrix combined with a number of shocked quartz clasts showing PDFs comprise 64 vol% (Fig. 8C). Most of the accreted altered silicate melt fragments have an angular, cuspate morphology (Fig. 8B). Some vesicular shards were observed (Fig. 8D). Trace amounts

TABLE 1. PLATINUM GROUP ELEMENT (PGE) COMPOSITIONS (NG/G) OF THE ACCRETIONARY LAPILLI AND THEIR HOST ROCK (BULK ROCK OF LOWERMOST SUBUNIT 3 WITHOUT ACCRETIONARY LAPILLI)

Sample	Ir	Ru	Pt	Rh	Pd
Accretionary lapilli	u.l.d.	u.l.d.	0.22	u.l.d.	0.31
Bulk rock	u.l.d.	u.l.d.	0.23	u.l.d.	0.19
d.l.	0.038	0.062	0.043	0.013	0.127
Cretaceous-Paleogene boundary clay*	0.83	1.57	1.37	0.22	1.84
Continental crust†	0.02	0.21	0.51	0.06	0.52

Note: d.l.—detection limit after Tagle et al. (2004); u.l.d.—under limit of detection. Rh values are from Peucker-Ehrenbrink and Jahn (2001).
*Composition of the El Guayal Cretaceous-Paleogene boundary clay (sample J) after Goderis et al. (2013).
†Composition of the continental crust after Wedepohl (1995).

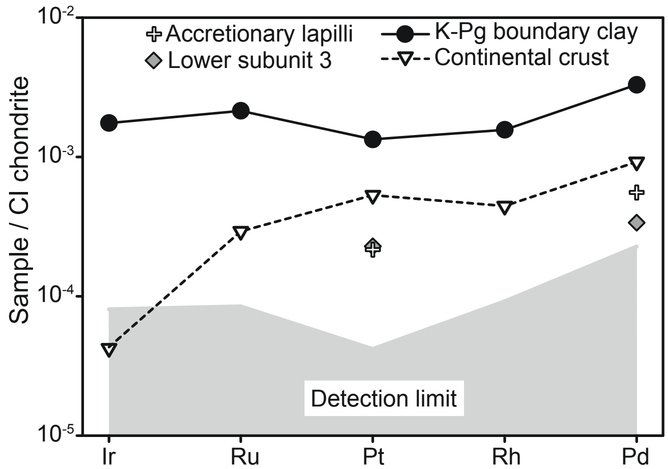

Figure 7. Carbonaceous chondrite (CI)–normalized platinum group element (PGE) concentrations of the accretionary lapilli and their host rock (bulk rock of lowermost subunit 3 without accretionary lapilli) compared to the composition of the El Guayal Cretaceous-Paleogene (K-Pg) boundary clay (Goderis et al., 2013) and the continental crust (Wedepohl, 1995; Rh values from Peucker-Ehrenbrink and Jahn, 2001). Detection limit (gray area) is from Tagle et al. (2004). CI composition is from Tagle and Berlin (2008).

of feldspar, apatite, titanite, ore minerals, and mica (locally intergrown with rutile) were observed using SEM-EDS.

Calcite Ejecta and Their Aggregates

Calcite particles with spherulitic to recrystallized microstructures and various aggregates with altered silicate melt were distinguished. Light microscopy studies showed particles with an internal spherulitic texture, which appear as fragmented lumps and fragments ≤2 mm in size as well as spheroids ≤250 µm in diameter. They contain voids <1 µm in diameter. In subunit 4, there are comparable smaller spheroids (~20–40 µm). The spherulitic microstructure is represented by radiating crystal growths, which, under crossed polarizers, yielded "feathery"-like extinction (Figs. 9A and 9C), or spheroids with a cross-like extinction (Figs. 4F and 9C). Recrystallization is characterized by a fine-grained, unoriented microstructure with locally larger crystal sizes (Fig. 9D) and occurs in individual ejecta particles. Recrystallization can also be observed at the rim of spherulitic particles. Both spherulitic and recrystallized particles contain different microstructures at their rim. These are represented by radially elongate to unoriented arranged crystals (arrows in Fig. 9D); these do not contain voids. Cathodoluminescence studies of spherulitic calcite particles and spheroids showed no or a reduced luminescence, with a dark red to dull brown color (Figs. 9E and 9F). Many recrystallized particles emitted a reduced, heterogeneous luminescence of brick brown to orange color, with lower intensities seen from locally larger crystals. At the rim of spherulitic and recrystallized particles, the coarser elongate crystals exhibited radially arranged, nonluminescent spikes (arrows in Fig. 9F). A bright yellow luminescence was observed from coarse-grained sparitic calcite that precipitated in pore space and most micritic calcite clasts.

Different carbonate-dominated aggregates can be distinguished: (1) spheroidal calcite aggregates within accretionary lapilli (Figs. 8B and 8E) and in the uppermost subunit 3 (Figs. 4E and 10A) that are composed of a vesicular silicate melt core with spherulitic to needle-like calcite at the rim; (2) calcite particles that are completely or partially coated with altered silicate melt (MP1; Figs. 5, 10B, and 10C; Supplemental Fig. S1) of various thicknesses (~1 µm to ~1 mm), where the associated calcite at the contact to the silicate melt has a recrystallized microstructure (Fig. 10D); and (3) larger aggregates with a diameter of 1.5 cm that were deposited together with the accretionary lapilli. These display distinct zonation, with recrystallized calcite at the center that is progressively replaced by silicate melt toward the rim (Fig. 10E; Supplemental Fig. S2). No calcite is present at the rim,

TABLE 2. COMPOSITIONS (wt%) OF SILICATE MELT PARTICLES (ALTERED TO CLAY MINERALS) IN THE BULK ROCK COMPARED WITH ALTERED SILICATE MELT FRAGMENTS IN ACCRETIONARY LAPILLI

Type:	High SiO_2, K_2O/low FeO, MgO		Low SiO_2, K_2O/high FeO, MgO	
Sample:	Bulk rock	Accretionary lapilli	Bulk rock	Accretionary lapilli
	SiO_2 > 52 wt%	SiO_2 > 50 wt%	SiO_2 < 37 wt%	SiO_2 < 41 wt%
N:	36	23	75	10
SiO_2	53.4 ± 0.9	52.5 ± 1.3	35.5 ± 0.8	38.3 ± 1.9
TiO_2	0.10 ± 0.07	0.28 ± 0.21	<0.09	0.16 ± 0.08
Al_2O_3	17.7 ± 1.1	17.0 ± 0.8	15.1 ± 0.7	14.4 ± 1.0
FeO	3.13 ± 0.74	2.45 ± 0.75	7.18 ± 0.93	7.81 ± 0.82
MgO	9.3 ± 2.6	12.0 ± 1.9	24.2 ± 3.5	22.5 ± 2.0
CaO	2.21 ± 0.69	1.56 ± 0.35	0.77 ± 0.30	1.10 ± 0.28
Na_2O	0.27 ± 0.16	0.28 ± 0.13	<0.06	0.15 ± 0.07
K_2O	1.90 ± 1.23	2.23 ± 0.66	0.13 ± 0.11	0.27 ± 0.15
Total	87.9 ± 2.4	88.2 ± 3.4	82.9 ± 3.6	84.7 ± 1.7

Note: N—number of analyses. The average compositions were obtained by selecting the analyses according to their SiO_2 content.

TABLE 3. RESULTS OF THE MODAL CONTENT (vol%) ANALYSIS OF EL GUAYAL UNITS BASED ON CHEMICAL MODELING OF ELECTRON MICROPROBE AND X-RAY FLUORESCENCE (XRF) ANALYSES

Subunit	Sample	Cal	Dol	CM	SiO_2	K-fsp	Hem	Total	*s* (±vol%)
1u	G04	74.4	19.7	4.9	0.6	0.5	n.m.	100.2	0.2
1u	G05	76.4	15.0	7.6	0.3	0.7	n.m.	100.0	0.2
2l	G06	73.4	6.0	16.1	4.1	0.8	n.m.	100.4	0.3
2m	G07	70.9	4.2	19.2	5.4	0.6	n.m.	100.3	0.3
2m	G08	63.8	n.m.	27.3	8.4	0.7	n.m.	100.3	0.4
3l	G09	54.8	8.2	32.7	4.7	0.3	n.m.	100.8	1.1
3l	G10	53.1	5.6	36.1	5.3	0.8	n.m.	100.8	0.9
3l	G11	58.6	n.m.	32.5	9.0	n.m.	n.m.	100.0	0.8
3m	G12	45.5	n.m.	47.6	7.0	n.m.	n.m.	100.0	1.3
3u	G14	24.4	n.m.	65.8	8.5	n.m.	2.1	100.9	0.8
3u	G13	32.8	n.m.	56.7	9.3	n.m.	2.3	98.8	0.9
4	G15	16.9	n.m.	59.2	21.3	n.m.	2.7	100.2	2.6
Acc. lapilli	G09/10L	10.7	6.2	18.5	64.3	0.1	n.m.	99.9	0.1

Note: Cal—calcite; Dol—dolomite; CM—clay minerals; SiO_2—quartz and silica; K-fsp—potassium feldspar; Hem—hematite; s—cumulative error (derived from the difference for each element between the calculated bulk rock composition and the XRF bulk rock composition). Suffix at subunit marks the stratigraphic level (l—lower; m—middle; u—upper). n.m.—not modelled.

and pseudomorph pore space dominates. The microstructure of the different zones in terms of the abundance of silicate melt, recrystallized calcite, and pore space is comparable to that seen in individual ejecta particles of MP2a (Figs. 4B and 5; Supplemental Figs. S3 and S4), indicating cogenetic formation conditions. (4) The last type is aggregates dominated by recrystallized calcite with quartz grains near the rim <125 µm in size, with (decorated) PDFs (arrows in Fig. 10F). Under crossed-polarized light, a characteristic texture of interlocking, internally fine-grained calcite patches can be recognized. These aggregates are associated with altered silicate melt around the particle, interstitial as layered elongated intercalations defining flow textures, or rounded inclusions. In this study, these particles will be termed MP2b.

DISCUSSION

Interpretation of the Petrographic and Chemical Data

The stratigraphic succession documents the different phases of arrival of impact ejecta on top of the basal monomict carbonate megabreccia (subunit 1). The silicate and calcite ejecta and their aggregates provide insights into their formation conditions and genetic relations during the impact processes (Table 4). When interpreting the petrographic and chemical data, sedimentary, impact, and alteration processes have to be considered.

Subunit 2

Implications from silicate melt particles. The presence of altered silicate melt particles in subunit 2 indicates the deposition of material from the lower excavation zone of the Chicxulub impact crater together with local sediments from high-density gravity flows. The melt particles were formed by adiabatic pressure release from shock pressures of >60–80 GPa and subsequent cooling from postshock temperatures of 1300–3000 °C (Stöffler, 1971; Engelhardt et al., 1995; French, 1998). MP1 resembles altered melt particles from suevites within the Chicxulub impact structure (e.g., Claeys et al., 2003; Hecht et al., 2004; Wittmann et al., 2004; Tuchscherer et al., 2005) and Cretaceous-Paleogene sites on the southern Yucatán Peninsula (Pope et al., 2005). The predominant flow texture in MP1 indicates plastic deformation upon cooling and argues for temperatures ≳750 °C (Wali, 1985; Fecker, 1993; Engelhardt et al., 1995). The rare, fragmented, vesicular, thin-walled altered silicate melts resemble shards derived from volcanic eruptions, such as fragments seen in pyroclastic flow deposits (Fisher and Schmincke, 1984), and they reveal that a solid state occurred before deposition in the water column.

The chemically heterogeneous clay mineral compositions indicate a succession of alteration processes in the silicate melt particles. The composition, with higher SiO_2 content, is comparable for many elements (MgO, FeO, K_2O) to that seen in altered impact melt particles from the Yaxcopoil-1 borehole (e.g., Hecht et al., 2004). The SiO_2-poor composition indicates a dissolving process, with silica release during pronounced alteration. This may have induced the silicification of fine-grained calcite particles and the coherent precipitation of sparitic calcite in the interconnected pore space. These processes can be considered as an important mechanism for cementing the ejecta deposits that act as a sealing facies above the oil-producing reservoir facies of the Cantarel oil fields in the Campeche marine platform (Grajales-Nishimura et al., 2000, 2009). This sealing effect may have been induced by a shorter-term alteration that probably started rather early; Kieffer and Simonds (1980) proposed that silicates may react with hot volatiles during ejecta transport to produce hydrated minerals such as clays. Results from experiments, and also observations of natural deposits related to nuclear waste deposits, at different time scales and settings than impact events,

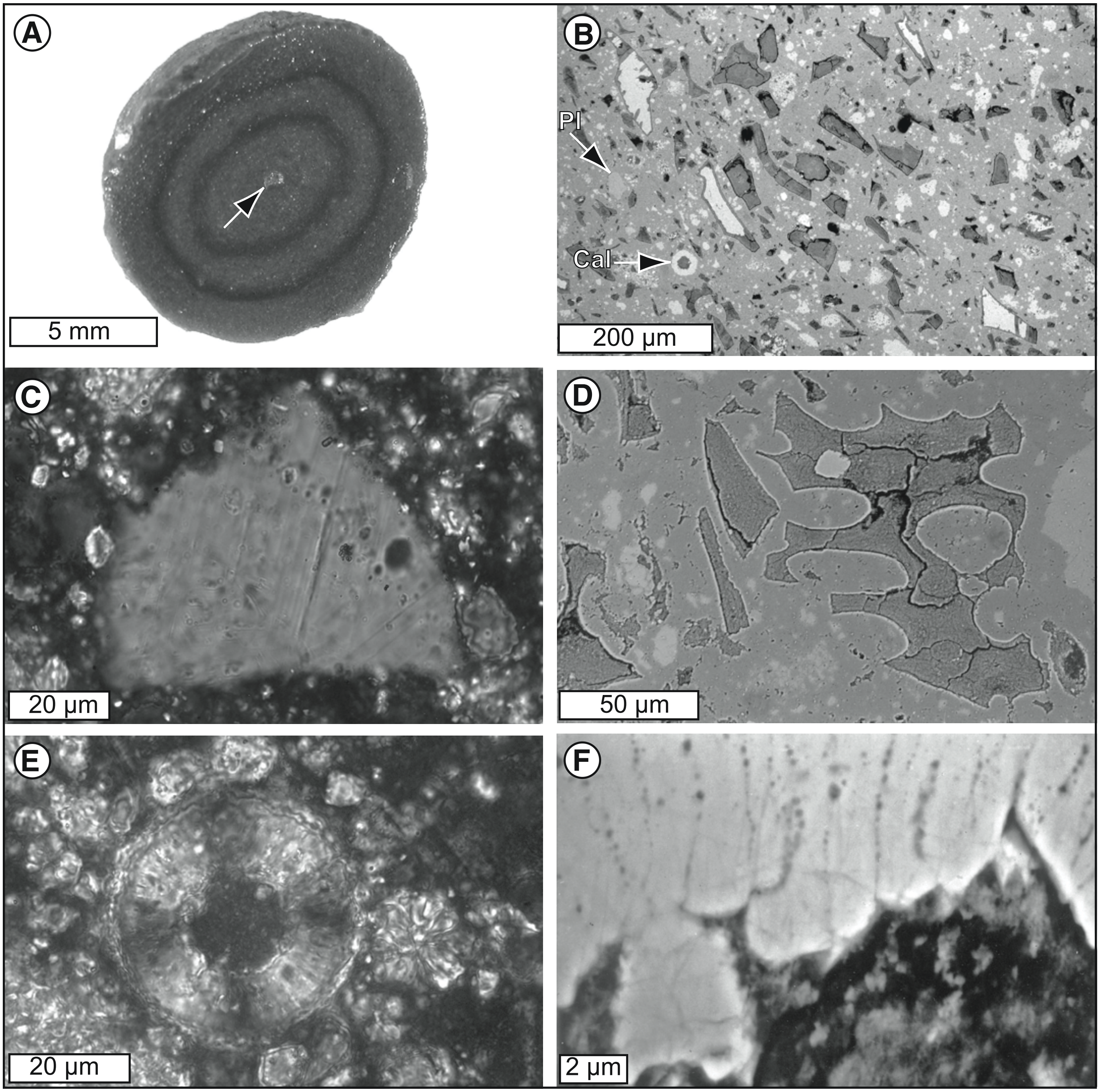

Figure 8. The structure of accretionary lapilli and their accreted particles. (A) Broken lapillus showing multiple concentric layers and nucleus (arrow). (B) Backscattered-electron (BSE) micrograph showing tangentially aligned particles dispersed in a matrix of silica. Bright—calcite; dark—altered silicate melt fragments; arrow—rare plagioclase (Pl). Cal with arrow—spheroidal calcite aggregate with a core of altered silicate melt (see also E, F). (C) Micrograph (cross-polarized light, XPL) of shocked quartz with multiple sets of planar deformation features. (D) BSE micrograph of altered silicate melt fragment with vesicular morphology. (E) Micrograph (XPL) of spheroidal aggregate composed of calcite with a radiating, needle-like microstructure and a nucleus of altered silicate melt. (F) BSE micrograph of spheroidal calcite aggregate showing voids between radiating subgrains.

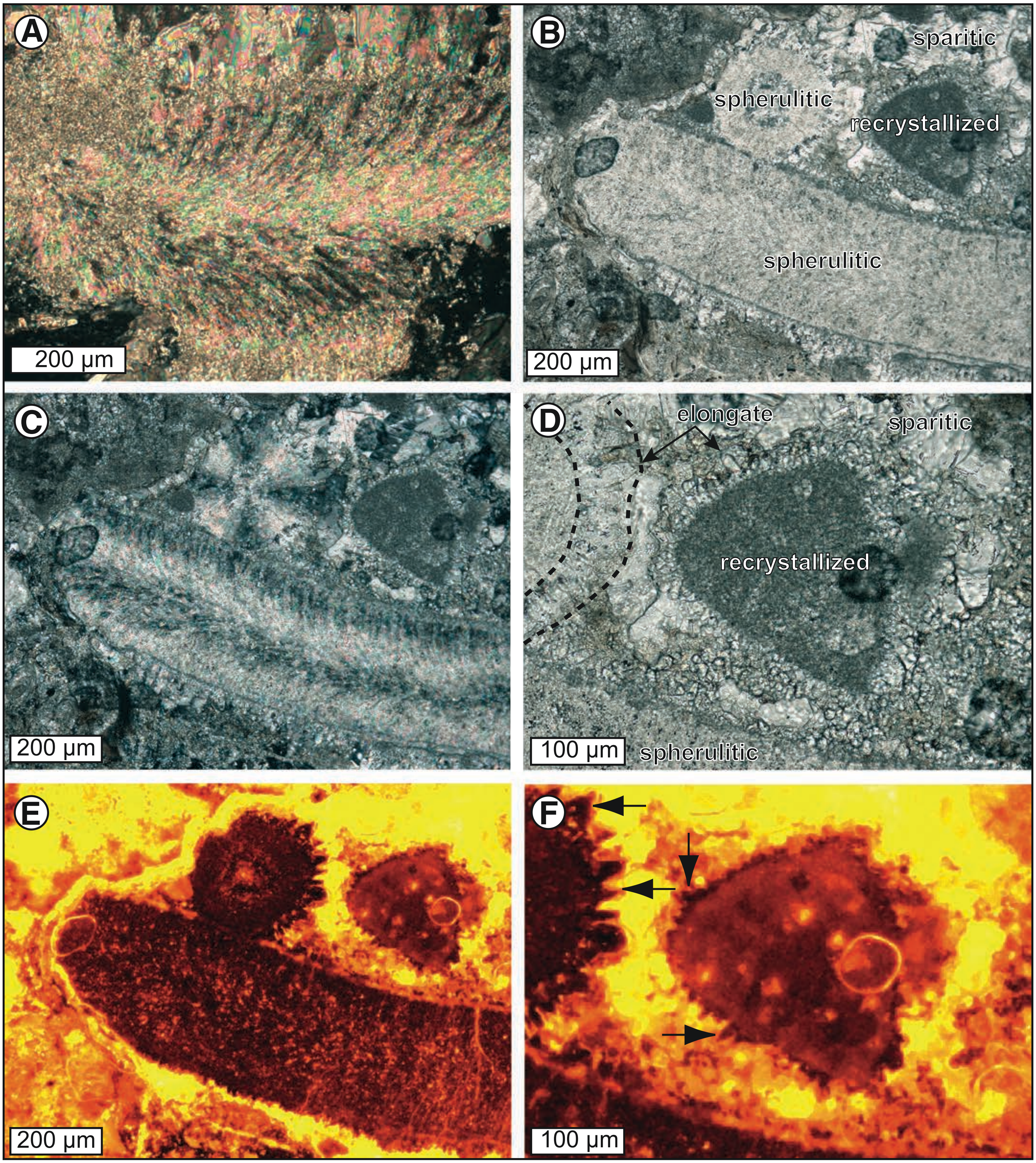

Figure 9. Transmitted light and cathodoluminescence (CL) micrographs of calcite microstructures in ejecta particles from lower subunit 3. (A, C) The spherulitic microstructure is represented under crossed polarizers by a “feathery”-like or cross-like extinction and no or reduced luminescence with a dark red to dull brown color (E). (B, D) The recrystallized microstructure occurs in individual ejecta particles and at the rim of spherulitic particles with reduced, heterogeneous luminescence (F). At the rim of spherulitic and recrystallized particles, radially elongated to unoriented arranged crystals (D) exhibit nonluminescent spikes (arrows in F). (A, C) Cross-polarized light. (B, D) Plane-polarized light. (E, F) CL. Bubble shapes in B–F are artifacts from preparation.

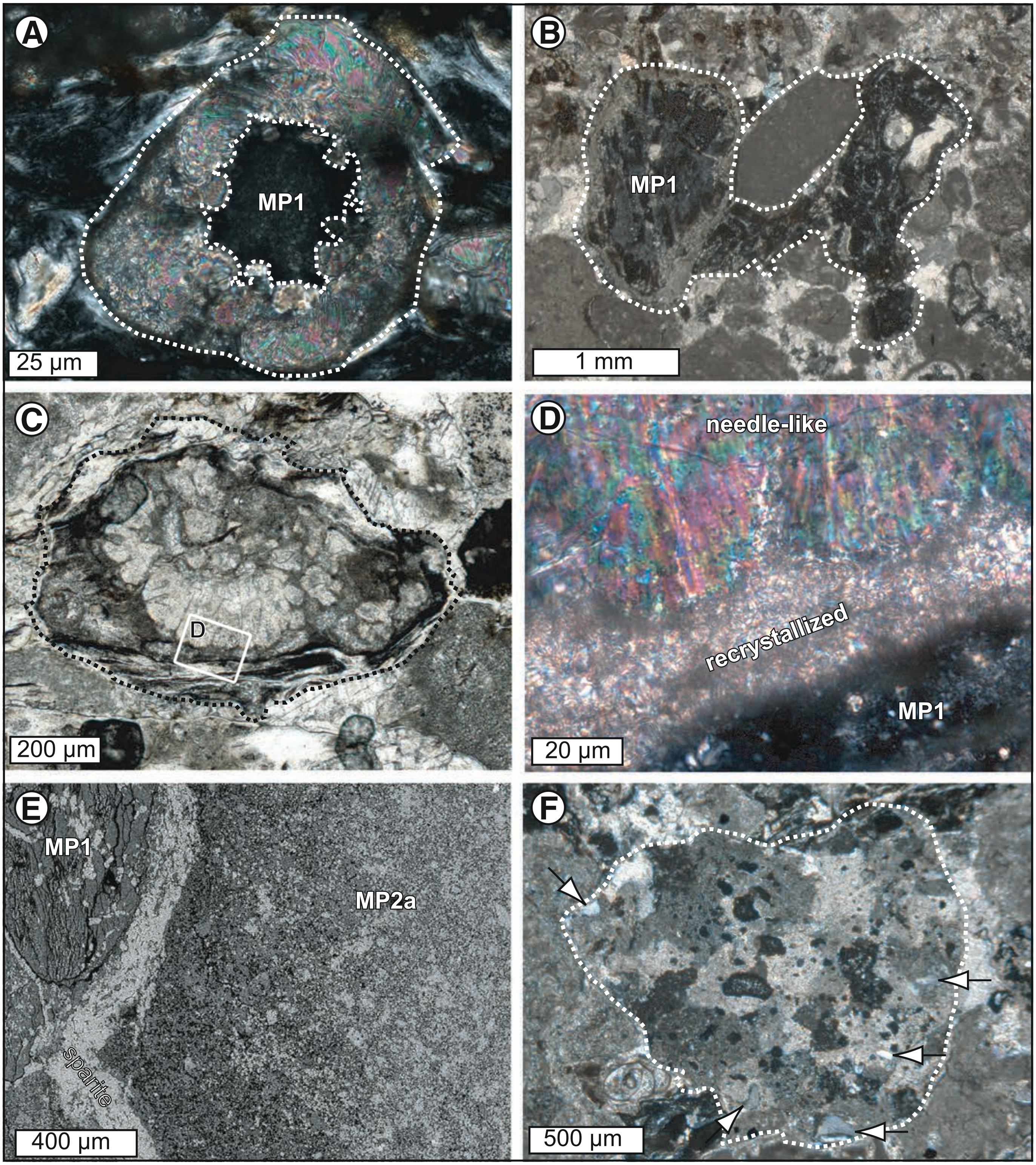

Figure 10. Transmitted light and backscattered-electron (BSE) micrographs of aggregates composed of calcite and silicate melt. (A) Spheroidal calcite aggregate with a vesicular nucleus of altered melt particle type 1 (MP1, uppermost subunit 3). Compare with Figure 8E. (B) Calcite clast that is partially mantled with MP1 (lower subunit 3). (C) Radially arranged, blocky calcite with "cauliflower" morphology and rim of MP1 (upper subunit 2). (D) Close-up of C showing a needle-like calcite microstructure at the center, and recrystallized calcite at the contact with the rim of MP1. (E) At the rim of a silicate melt–coated calcite particle (1 × 2 cm, lower subunit 3), recrystallized calcite is progressively replaced by altered silicate melt and associated with pseudomorph pore space (see also Supplemental Fig. S2 [see text footnote 1]). (F) Melt particle type 2b (MP2b, lower subunit 2) with a characteristic calcite microstructure of interlocking, internally fine-grained patches and rounded inclusions of silicate melt. Arrows show quartz grains <125 µm in size near the rim. (A, B, D, F) Cross-polarized light. (C) Plane-polarized light. (E) Backscattered-electron micrograph. Dark bubble shapes in C are artifacts from preparation.

however, provide further insights. These studies have shown that the dissolution of borosilicate glasses (Geisler et al., 2010) and clay minerals (Pusch, 2000) by hot water and water vapor can initiate the precipitation of silica and cementation, as described (Couture, 1985a, 1985b; Pusch and Karnland, 1988; Pusch et al., 1991, 1993; JNC, 2000).

Implications from spherulitic and recrystallized calcite particles. The spherulitic calcite particles resemble "feathery" carbonate melt particles from the suevite of the Y6 borehole (Jones et al., 2000; Claeys et al., 2003) and the UNAM-7 borehole (Salge et al., 2019). The spherulitic calcite spheroids of El Guayal are similar to radially fibrous calcite spheroids from the diamictite bed of Albion Island that were interpreted to have formed by quench crystallization from carbonate melt (Ocampo et al., 1996). The reduced luminescence observed for the spherulitic calcite particles at El Guayal is similar to that observed for carbonate melt particles from the Y6 suevite (Heuschkel et al., 1998) and for ejecta deposits from northeastern Mexico (Schulte and Kontny, 2005). Similar fibrous structures may also occur in molluscs or brachiopod shells. The presence of spherulitic spheroids in subunit 4, where no microfossils were observed in one thin section, suggests an impact origin. This assumption is supported by the association of the spherulitic microstructure at El Guayal with nonluminescent elongate and recrystallized microstructures. A cogenetic relationship for the spherulitic, recrystallized, and elongate microstructure is indicated by the reduced luminescence, which is different from the bright luminescence observed for the coarse-grained sparitic calcite that precipitated within pore space. These observations support the interpretation that the spherulitic calcite particles at El Guayal may represent carbonate melt particles that were ejected from depths of a few hundred meters in an originally liquid state (T > 1240 °C, P > 30 bar; Ivanov and Deutsch, 2002) and quenched with very high cooling rates of $\Delta T > 100s\ °C\ s^{-1}$ (Fig. 3; Jones et al., 2000). The pressure of the overlying target rock would inhibit the decomposition reaction during decompression at constant pressures. The small voids in spherulitic calcite particles that were also observed at the UNAM-7 borehole may have formed during crystallization at disequilibrium related to a vapor phase (Salge et al., 2019).

The recrystallized and elongate microstructures with reduced luminescence at the rims of spherulitic carbonate melt particles may reveal different formation conditions during the impact process. The recrystallized microstructure at the rim of spherulitic carbonate melt particles may indicate the subsequent modification of quenched carbonate melts by short but intense thermal stress during atmospheric transport. The progression of microstructures from fine-grained, recrystallized to larger elongate structures toward the rim of spherulitic carbonate melt particles may indicate crystallization at a lower cooling rate of ΔT ~10–100 °C s^{-1} (Fig. 3; Jones et al., 2000). As a consequence, the abundant recrystallized calcite ejecta particles may not have exclusively formed from melts. They could also represent unmolten ejecta particles that were emplaced at low shock pressures and then thermally modified during atmospheric transport. This assumption is supported by large, up to 25-cm-diameter, carbonate ejecta represented by polished, striated rounded pebbles from the Cayo district (475 km southeast of the Chicxulub crater; Ocampo et al., 1997a; Kletetschka et al., 2020). The Pook's Pebbles reveal electric discharge signatures that indicate electric discharge taking place during the formation of the fluidized ejecta

TABLE 4. CLASSIFICATION OF SILICATE AND CALCITE EJECTA AND THEIR AGGREGATES

Classification	Formation condition	Genetic relation during impact process
Spherulitic calcite	Carbonate melts formed at pressure (P) > 30 bar and temperature (T) > 1240 °C. Quenching at a high cooling rate of $\Delta T > 100s$ °C s^{-1}. Voids by crystallization at disequilibrium related to a vapor phase.	Carbonates at depths larger than several hundred meters were shocked to high shock pressures. Rapid quenching during ballistic transport.
Recrystallized calcite	Short, intense thermal stress.	Emplacement by ballistic transport and/or secondary cratering of carbonates shocked to low shock pressures. Atmospheric transport at moderate to high temperatures.
Elongate calcite	Prolonged thermal stress with a low cooling rate of ΔT ~10–100 °C s^{-1}.	Prolonged atmospheric transport at moderate temperatures.
Melt particle type 1	Plastic deformation at $T \gtrsim 750$ °C.	Prolonged atmospheric transport at high temperatures. Reaction with volatiles may have initiated postdepositional silicification and cementation.
Shards	Fragmentation of solidified melts.	Explosive-like interaction of hot melt with water and rapid quenching.
Melt particle type 2	Aggregation of hot silicate melts with relatively cold, weakly shocked sediments. Amalgamation at $T \gtrsim 750$ °C induced recrystallization and partial dissociation of calcite.	Consolidation of a hot suevitic component from lower target lithologies with sediments from upper target lithologies during prolonged atmospheric transport. Dissociation of calcite sustained gas-driven transport.
Spheroidal aggregates	Aggregation of liquid carbonate melts with solid silicate melt.	Consolidation of the finest fraction of a solid suevitic component with liquid carbonate melts during atmospheric transport.
Accretionary lapilli	Aggregation of solid particles in a steam-condensing environment at T ~100 °C. Recurring exchange with a hotter environment. Formation of calcite matrix possible by exothermic (change in enthalpy ΔH = –178 kJ/mol) back-reactions of CaO with CO_2 (and H_2O).	Turbulent mixing of the finest fraction of ejecta in volatile-rich, high-density currents. Prolonged association of two environments with different temperatures. Prolonged energy release and delayed water vapor release by back-reactions of dissociated carbonates and sulfates.

blanket (Kletetschka et al., 2020). At the rim of some Pook's Pebbles, a recrystallized microstructure is represented by faint, mostly annealed grain boundaries of calcite subgrains ~1 µm in size, which resembles the recrystallized calcite microstructure observed at El Guayal. The surface features of the Pook's Pebbles were interpreted by Kletetschka et al. (2020) to have formed at localized extreme pressures and temperatures during transport through a near-surface cloud.

Aggregation of silicate melt with carbonates. At El Guayal, the radially arranged, blocky calcite cores with "cauliflower" morphology in silicate melt–coated aggregates are similar to quenched carbonate melt aggregates in ejecta deposits in northeastern Mexico (Schulte et al., 2003; Schulte and Kontny, 2005). Their needle-like microstructure implies quenching at intermediate cooling rates of $\Delta T \sim 100$ °C s^{-1} (Fig. 3; Jones et al., 2000). The recrystallized microstructure between the quenched calcite core and the silicate melt suggests modification during aggregation by heat transfer from silicate melt.

MP2a is interpreted to have formed by accretion of hot, viscous silicate melts with carbonate ejecta. During amalgamation, euhedral calcite microcrystals may have formed at low cooling rates within a silicate melt matrix. This assumption is supported by the silicate melt–coated calcite aggregates ~1.5 cm in size in the lower subunit 3, where the different zones with respect to the abundance of silicate melt, recrystallized calcite, and pore space correspond to the variations in MP2a. A solid, unmolten state of calcite during amalgamation is indicated by the presence of degraded microfossils. Similar observations were also made for ejecta particles from northeastern Mexico where benthic foraminifera are enveloped by silicate melt (Schulte and Kontny, 2005). The pseudomorph pore space in MP2a, which is associated with microcrystalline calcite, is an indication for a displacement reaction of former calcite. The decomposition of calcite by hot silicate melt or transport of the particle into a hot environment has to be considered. The silicate melt is then able to modify the enclosed calcite. The lower temperature can be inferred by the silicate melt to glass transformation temperature (680–750 °C; Wali, 1985; Fecker, 1993), which is in a similar range to the calcite decomposition temperature. The optimum temperature of the calcination reaction ($CaCO_3 \Rightarrow CaO + CO_2$, change in enthalpy $\Delta H = 178$ kJ/mol) at traditional industrial lime kilns is 900 °C (Moropoulou et al., 2001). Free-surface and powder bed calcite decomposition experiments show that this reaction can already be observed between 660 °C and 740 °C (Beruto et al., 2004).

The microstructure of interlocking, internally fine-grained calcite patches in MP2b resembles that observed at the Yaxcopoil-1 borehole (Tuchscherer et al., 2004a). The arrangements of silicate melt in MP2b as rounded inclusions or elongate intercalations with calcite imply a plastic deformable state of both components. This is further supported by accreted, shocked quartz grains within the rim of MP2b. Experiments have confirmed that nominally brittle limestone can be plastically deformed in low-stress collision interactions under medium to high temperatures of ~175–625 °C and low pressures (Ocampo et al., 1997b).

The aggregates at El Guayal suggest formation in a hot regime, where relatively cold carbonate particles from upper target lithologies were strongly heated by the thermal energy of the superheated silicate melt. The lower temperature range of this regime may have been below the calcite decomposition temperature due to the presence of fossil-bearing calcite aggregates at El Guayal. This is consistent with the deposition temperature of ~600 °C for the suevite of the Nördlinger Ries crater (Stöffler et al., 2013, and references within). The upper temperature limit of this regime may be represented by the glass transformation temperature of melt particles around 680–750 °C (Wali, 1985; Fecker, 1993). The lack of crystallites in the altered silicate melt at El Guayal indicates that temperatures may have locally exceeded 1100 °C (Engelhardt et al., 1995).

Subunit 3

The presence of accretionary lapilli in subunit 3 indicates impact material derived from a later stage of the plume evolution that was deposited with local sediments from gravity or tsunami surges. A pronounced intermixing of the carbonate and silicate target lithologies in the ejecta plume is indicated by the higher abundance of MP2a and the presence of spheroidal calcite aggregates in both the upper subunit 3 and the accretionary lapilli. The latter are interpreted as accretionary carbonate melts, where the vesicular morphology of the silicate nucleus indicates its solid state upon coating with the carbonate melt. A former liquid state of calcite is indicated as previously argued by (1) the radially arranged, needle-like microstructure (Fig. 3; Jones et al., 2000); (2) the voids between the radiating calcite crystals; and (3) the reduced luminescence, which also can be observed for the spherulitic calcite particles.

In upper subunit 3, the predominantly recrystallized calcite particles suggest prolonged thermal alteration. The lack of calcite and the dominant presence of pseudomorph pore space in MP2a in the uppermost subunit 3 are interpreted to indicate complete calcite decomposition. Here, the thermal alteration would have been most effective for small particles due to their prolonged residence time in the hot ejecta plume.

Accretionary lapilli—aggregation at specific conditions. The accretionary lapilli are similar to volcanic accretionary lapilli with respect to (1) the accreted particle size of <150 µm, and in rare cases <300 µm, with a few nuclei of ~1 mm; (2) the tangential alignment of elongate particles; and (3) the multiple concentric zones due to differences in grain size. In impact-induced accretionary lapilli of the Nördlinger Ries crater (Graup, 1981), a tangential particle alignment and decreasing particle size near the rim have been reported. A similar tangential alignment of shard-like particles has been observed in accretionary coatings around glass and lithic cores at the Sudbury impact structure (Muir and Peredery, 1984). The presence of shocked minerals was also observed in accretionary lapilli from the upper Devonian Alamo breccia (Warme et al., 2002) and those related to the Sudbury impact event (Addison et al., 2005). Accretionary lapilli with multiple concentric zones due to smaller grain sizes were reported at the

Sudbury impact structure (Huber and Koeberl, 2017). Comparison with accretionary lapilli from other impact craters shows a deposition at stratigraphic levels that are comparable to El Guayal. In the case of the Sudbury impact structure, at a distance of 480–875 km from the crater center, accretionary lapilli are in the middle or upper parts of ejecta deposits (Addison et al., 2005; Huber and Koeberl, 2017). The Bosumtwi impact structure shows an accretionary lapilli unit on top of impact breccias (Koeberl et al., 2007). At the Nördlinger Ries crater, accretionary lapilli are on the top of graded suevite of the Deiningen 1001 and Nördlingen 1973 drill holes (Graup, 1981; Meyer, 2012).

The similarities of impact-generated and volcanic accretionary lapilli suggest that aggregation occurred under broadly similar conditions despite the significant differences in source conditions (Mueller et al., 2018). Experimental investigations of formation mechanisms for volcanic accretionary lapilli demonstrated that growth is controlled by collision of liquid-coated, solid, or molten ash-sized particles in a turbulent environment (Gilbert and Lane, 1994; Schumacher and Schmincke, 1995). Particle binding occurs as a result of surface tension forces of condensing liquids and by secondary mineral growth. These mechanisms and conditions allow accretion of a large number of individual particles in the form of concentric layers in a plume-like environment. Other possible mechanisms to create concentric layers in aggregates are electrostatic attraction between charged ash particles without the presence of a liquid phase (James et al., 2002; Telling and Dufek, 2012) or processes comparable to the formation of hailstone (Rose et al., 1995). The coherent deposition of the El Guayal accretionary lapilli together with aggregates formed by amalgamation of hot silicate melts with cold, likely water-saturated sediments suggests formation in relation to a steam-condensing environment at moderate to hot temperatures. The coherent formation of the accretionary lapilli and the upper ejecta deposits is evident from the petrographic and chemical results, including (1) the comparable PGE and trace-element concentrations of the accretionary lapilli and their host rock; and (2) the presence of spheroidal calcite aggregates both within the accretionary lapilli and in the uppermost subunit 3. Schulte and Kontny (2005) suggested that the turbulent mixing and heating of seawater during crater-outward movement of the ejecta curtain may have formed accretionary lapilli by providing large amounts of vapor in the ejecta curtain or plume. The steam-condensing environment implies moderate temperatures (~100 °C), which is consistent with the observation that most of the silicate melt particles are in form of solidified, fractured shards.

The multiple concentric zones of the El Guayal accretionary lapilli demonstrate changing environmental conditions in the ejecta plume. For volcanic accretionary lapilli, the concentric zones of different grain size are due to differences in the supply of particle sizes, which are related to a progressive increase in formation temperature in the ash plume (Gilbert and Lane, 1994). This temperature increase reduces the humidity and the amount of condensed liquid layers on particles, so that accretion is biased toward smaller grain sizes (Moore and Peck, 1962). In volcanic events, the collapse of a vertical eruption column can form hot, gaseous, particulate density currents known as pyroclastic flows (Fisher and Schmincke, 1984). Volcanic accretionary lapilli with multiple laminations are reported from ignimbrite flow units and their coignimbrite ash cloud deposits (e.g., Riley and Leat, 1999; Brown et al., 2010). The latter form by elutriation of fine ash from the moving pyroclastic flow. Consequently, the multiple laminations of the El Guayal accretionary lapilli likely recorded a recurring heat increase by the circulation from a steam-enriched, condensing environment with moderate temperature (~100 °C) to a hotter area of the ejecta plume. These observations signify prolonged formation and atmospheric residence time during a late stage of ejecta plume evolution.

Branney and Brown (2011) studied the threefold sequence in the 4–10.5-m-thick impact ejecta blanket of Stac Fada, Scotland, where a lower suevite unit grades into suevite with accretionary lapilli, which is in turn overlain by a thin layer of clast-supported dust pellets. These authors proposed a stratified density current similar to pyroclastic density currents. It was composed of a ground-hugging component of granular fluid passing up into less concentrated, more turbulent levels and a buoyant, dilute upper component. In the buoyant plume, dust aggregated into pellets. These dropped into a lower, more turbulent level of the density current and evolve into accretionary lapilli where ongoing circulation could form multiple laminations. The occurrence of pellet-like spheroidal calcite aggregates at El Guayal in both the upper subunit 3 and within accretionary lapilli supports this model. The lack of an impactor component in the El Guayal accretionary lapilli and their host rock suggests formation without contribution of material transported to the stratosphere as suggested by Huber and Koeberl (2017). The silicate-binding agent model (Johnson and Melosh, 2014), where molten silicate, or any condensable material, acts as a binding agent in the environment of the ejecta curtain that contains no water or atmosphere, is not applicable because the El Guayal accretionary lapilli formed during a late stage of the impact process, and the main matrix component was former calcite that had been diagenetically replaced by silica (Griscom et al., 1999; this study). The condensation of $CaCO_3$ from a gas phase into a liquid phase is not possible because $CaCO_3$ would decompose into solid CaO and CO_2 gas during decompression at constant temperature. The melt fuel-coolant interaction (MFCI) of an impact melt sheet with water (Grieve et al., 2010; Stöffler et al., 2013; Artemieva et al., 2013; Osinski et al., 2019) is supported by the predominant occurrence of silicate melt fragments in the El Guayal accretionary lapilli. It is, however, unclear how the pronounced intermixing of calcite ejecta with hot silicate melts in aggregates that were deposited with the El Guayal accretionary lapilli can be explained by this model.

Subunit 4

Subunit 4 is comparable with Cretaceous-Paleogene boundary sites around the world with respect to its enrichment of PGEs (Goderis et al., 2013) and the occurrence of shocked quartz (Claeys et al., 2002). The shocked quartz particles in subunit 4 of El Guayal show less decoration of their PDFs when compared to those in the underlying ejecta units. This may indicate a less intense thermal alteration of shocked quartz during emplacement. The size of spherulitic calcite spheroids in subunit 4 is in a similar range to calcareous dinoflagellates, the latter of which are common at Cretaceous-Paleogene ejecta sites (e.g., Wendler and Willems, 2002) and are also observed at the base of the postimpact sedimentary section of IODP-ICDP Hole M0077A (Gulick et al., 2017b). The microstructure of the spherulitic calcite spheroids, however, is different from calcareous dinoflagellates and resembles the larger 250 µm carbonate melt spheroids in subunit 3 and the spheroidal calcite aggregates in accretionary lapilli. These observations suggest a cogenetic relationship; consequently, subunit 4 represents the finest fraction of Chicxulub ejecta mixed with a small proportion of an extraterrestrial component.

The settling time in the water column can be calculated by assuming a maximum water depth of 200 m at the Yucatán shelf (Smit, 1999; Grajales-Nishimura et al., 2000) and applying the settling velocity of the particles present in subunit 4. Particles with maximum size of ~64 µm are observed, which corresponds to a settling velocity of 19 m/h (Smit et al., 1996) and settling time of ~10 h. To this time, the atmospheric residence time of supposedly several days to weeks has to be added. This time is short compared to marine sedimentation rates, and consequently few marine carbonates were incorporated into subunit 4.

Genetic Relationship of El Guayal Impactites to Chicxulub Crater Suevites and Proximal to Intermediate Cretaceous-Paleogene Sections

The polymict ejecta sequence from El Guayal contains local sediments and was partially reworked by tsunami currents; however, for most elements, its chemical signature matches the suevite drilled within the Chicxulub crater (e.g., Claeys et al., 2003; Schmitt et al., 2004; Tuchscherer et al., 2004b). Compared to the El Guayal ejecta deposit, the crater suevites have much higher K_2O and Sr concentrations (Fig. 6). This is attributed to prolonged alteration of the crater suevites by hydrothermal fluids, which were associated with the underlying hot melt pool (e.g., Ames et al., 2004; Hecht et al., 2004; Zürcher and Kring, 2004; Nelson et al., 2012). The chemical signatures, petrographic observations, and modal content indicate that such processes were not effective at El Guayal due to the deposition in a marine environment.

The cooling history can be inferred from petrological observations at the different sites. Spherulitic carbonate melt particles were only observed in the crater at the Y6 borehole in the upper part of the suevite (Claeys et al., 2003) and in the evaporite-rich megabreccia at the UNAM-7 borehole near the outer crater rim (Salge et al., 2019). Apparently, spherulitic carbonate melts are only preserved in impactites that were transported in the ejecta curtain or plume, where the conditions for the required high cooling rates existed. In contrast, the deposition in ground-surged suevite close to high-temperature melt layers with prolonged hydrothermal activity excluded rapid quenching.

At El Guayal, the link between the global Cretaceous-Paleogene boundary and the Chicxulub impactites is marked by the projectile component (chemically identified by the PGE enrichment; Goderis et al., 2013) together with Chicxulub ejecta (shocked quartz, carbonate melt spheroids) in subunit 4. Both the enrichment of PGEs and the shocked quartz observed in subunit 4 of El Guayal are similar to the dual-layer stratigraphy at intermediate Cretaceous-Paleogene sites 2000–4000 km away from Chicxulub (e.g., Bohor et al., 1987; Izett, 1990; Schulte et al., 2009, 2010).

The various aggregates in ejecta deposits from the Chicxulub crater on the southern Yucatán Peninsula (Pope et al., 1999, 2005; Fouke et al., 2002) and as far as northeastern Mexico (Schulte et al., 2003, 2012; Schulte and Kontny, 2005), Texas and New Jersey (Schulte et al., 2006; Yancey and Guillemette, 2008), and Cuba (Alegret et al., 2005) lack the clear associations with accreted shocked quartz and altered silicate fragments that are commonly observed at El Guayal. At the ejecta deposits of Armenia, Belize (Figs. 1 and 11), at ~470 km from the crater center (Pope et al., 2005; King and Petruny, 2015), spheroids of coarse detrital calcite grains with a rim of fine calcite particles, and in some cases with an altered silicate melt nucleus, resemble accretionary lapilli. Compared to the much larger El Guayal accretionary lapilli, the spheroids from the Armenia site contain no shocked quartz, and silicate melt particles are rare. This indicates formation during an early stage of the impact process when silicates from the lower excavation zone were not abundant. Johnson and Melosh (2014) have shown that accretionary lapilli can form within the ejecta curtain early in the ejection process, well before reentry into an atmosphere or ballistic emplacement. The overlying reworked conglomerate present at the Armenia site (composed of micritic limestone, melt particles, shocked quartz, and accretionary lapilli; Pope et al., 2005; King and Petruny, 2015) is only briefly described. However, due to the similar components compared to the ejecta sequence at El Guayal, both units could have been emplaced by similar processes.

The calcite microstructures and their association with altered silicate melt and porosity in MP2a are similar to the accretionary calcite aggregates that are composed of micron-sized calcite subgrains and contain various amounts of larger clay masses with heterogeneous compositions (Schulte et al., 2006, 2009, 2010, 2012; Yancey and Guillemette, 2008). Yancey and Guillemette (2008) interpreted the aggregate microstructure to have formed by accretion of small solid particles and suggested an origin from carbonate crystals generated within the Chicxulub ejecta plume. A formation by aggregation of individual carbonate crystals is unlikely for MP2a due to the presence of degraded microfossils; however, this scenario may be possible for the former calcite matrix in the El Guayal accretionary lapilli. Yancey and Guillemette (2008) discussed the possibility that minute calcite crystals may form by back-reactions from decomposed $CaCO_3$. Solid CaO can combine directly with CO_2 gas at higher temperatures, whereas at lower temperatures, it can react with H_2O to produce $Ca(OH)_2$ in the CO_2-enriched ejecta plume, and then $Ca(OH)_2$

can react with CO_2 to form $CaCO_3$ and water vapor (Agrinier et al., 2001). Formation by back-reactions has also been suggested for microcrystalline calcite in carbonate layers that were deposited close to the impact crater in the aftermath of the impact event (Bralower et al., 2020).

In summary, pronounced intermixing of silicate melt with carbonate is only observed at El Guayal and at more proximal to intermediate Cretaceous-Paleogene sites, but not at ejecta deposits on the southern Yucatán Peninsula. These observations document an enrichment in silicate melt during the late stage of ejecta plume evolution and enhanced mixing of the silicate and sedimentary target rock during prolonged atmospheric transport.

CONCLUSIONS

Petrographic and chemical studies of the Cretaceous-Paleogene boundary sequence at El Guayal show the deposition of ejecta with local sediments from gravity or tsunami surges on top of a monomict carbonate megabreccia. The ejecta units are progressively enriched in altered silicate melt and topped by a Cretaceous-Paleogene boundary clay layer with a projectile component (Goderis et al., 2013). The occurrence of potential carbonate melt particles with a spherulitic microstructure indicates rapid cooling during ejection. Their cogenetic association with recrystallized microstructures and elongate calcite crystals reflects variations in the cooling rates in an ejecta plume with a heterogeneous temperature distribution. The recrystallized microstructure may indicate short but intense thermal stress at postshock, high-temperature conditions during airborne transport. Various aggregates of silicate melts and calcite document particle-particle interactions and intermixing of components from lower and upper target lithologies in different environments. Aggregates of recrystallized calcite with altered silicate melt indicate amalgamation of viscous silicate melt with carbonate at elevated temperatures. Hence, the presence of pseudomorph pore space in these aggregates suggests the decomposition of euhedral calcite microcrystals at temperatures of ≳750 °C. Accretionary lapilli with multiple concentric zones of smaller aggregated particles suggest formation in a turbulent, steam-condensing environment at moderate temperature of ~100 °C with recurring exchange to a hotter area of the ejecta plume.

Based on the results obtained in this and previous studies, five distinct stages can be reconstructed for the evolution, deposition, and alteration of the Chicxulub ejecta blanket:

(1) In the high-pressure zone between the impactor and the sedimentary target, carbonate and sulfate decomposition products (CaO, MgO, CO_2, SO_x) were ejected at high velocity and formed an initial vapor flow (Fig. 12A). Steam explosions from instantly vaporized target water led to flow-like transport processes (Pope et al., 2005).

(2) Anhydrite and carbonate megablocks were excavated out of the impact crater and initiated a laterally extending, ground-

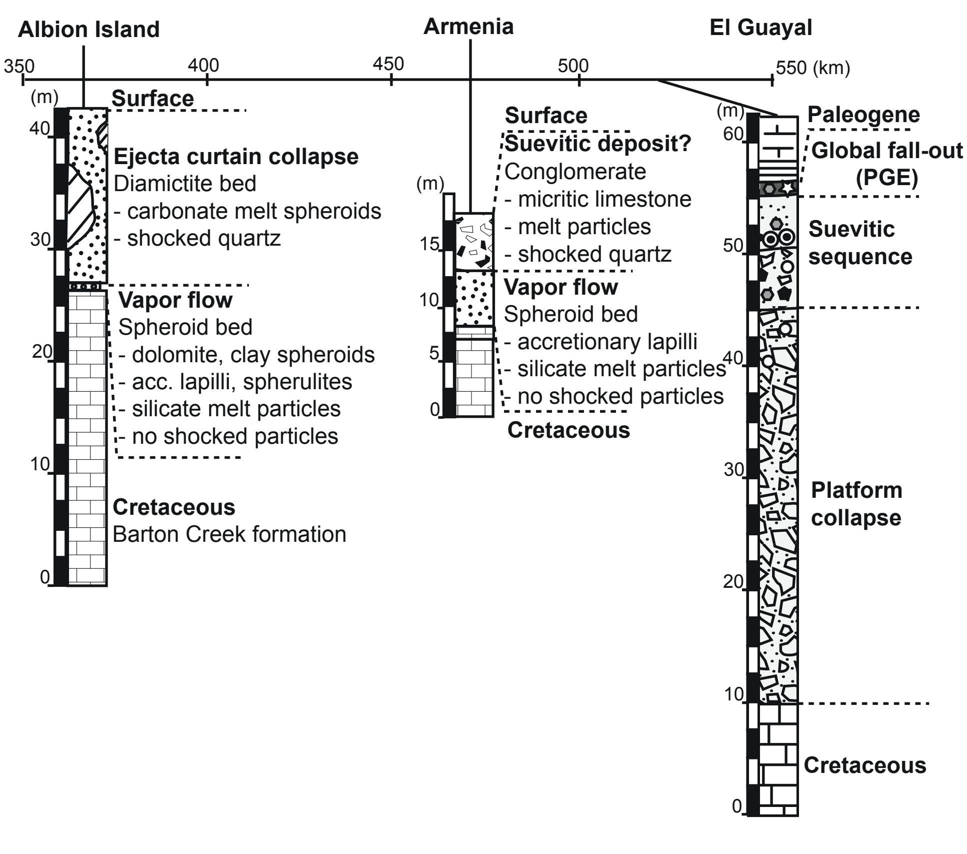

Figure 11. Stratigraphic comparison of the marine Cretaceous-Paleogene site at El Guayal, Tabasco, Mexico, with subaerially exposed ejecta deposits at Albion Island and Armenia, Belize, on the southern Yucatán Peninsula in relation to the radial distance to the Chicxulub crater center (modified from Pope et al., 1999, 2005; Schulte et al., 2010). PGE—platinum group element. Legend as in Figure 2.

hugging surface flow (Pope et al., 2005; Kenkmann and Schönian, 2006). Carbonates buried at depths larger than a few hundred meters were ejected out of the impact crater in an originally liquid state (Jones et al., 2000). The presence of water vapor sustained the transformation from a ballistic transport to a lateral flow regime. Thereby, small amounts of silicate melts from lower target lithologies were injected into the outward-expanding, carbonate-dominated ejecta curtain.

(3) A turbulent expanding ejecta plume was formed above the impact crater. With increasing excavation depths, the ejecta plume was enriched in shocked and molten components of the crystalline basement. About several tens of minutes after the impact, the ejecta plume partially collapsed (Fig. 12B). The vaporized and condensed material derived from the projectile and target rock was lifted to the stratosphere for mostly global distribution. Molten and solid target rock fell back to the surface. Thereby, hot silicate components were mixed with the fine fraction of local surface-derived sediments, of which the latter were displaced by the preceding ejecta curtain. The fusion of porous, water-saturated sediments with hot silicate melt resulted in additional release of vapors during dissociation of sediments. These processes sustained a gas-driven, lateral basal transport, similar

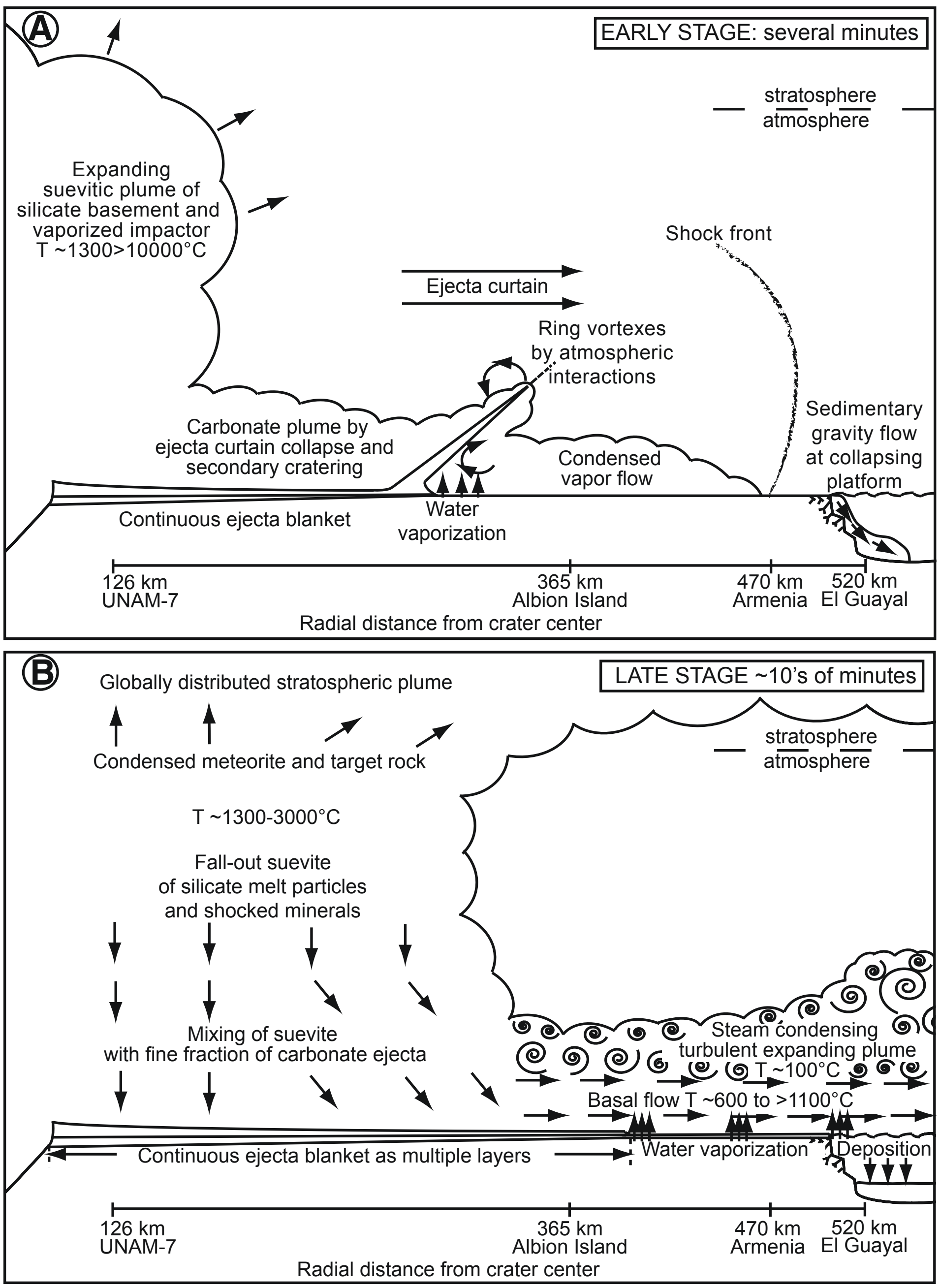

Figure 12. Model of Chicxulub ejecta plume during (A) early stage and (B) late stage. A final crater diameter of ~200 km is assumed, and crater modification processes are not shown. Not to vertical scale.

to a volcanic pyroclastic flow, with locally varying temperatures of ~600 °C to >1100 °C.

At a higher level, this basal flow was accompanied by a highly turbulent plume similar to volcanic coignimbrite ash clouds. This zone is inferred to have had a moderate temperature (~100 °C) due to admixing of ambient air. Thereby, steam condensed and accretionary lapilli were formed from the fine fraction of carbonate and silicate material that emerged from the basal flow, a process referred to as elutriation in a volcaniclastic environment. Due to the close association of the hot basal flow with a turbulent ash plume of moderate temperature, the accretionary lapilli and the fine fraction of ejecta particles circulated several times between the moderate- and hot-temperature regimes. Progressive lapilli growth ultimately led to aggregates that became too heavy to be held in suspension by the flow. Consequently, the accretionary lapilli settled and sank through the water column near the area now represented by the El Guayal site. This scenario is similar to coignimbrite ash clouds associated with volcanic pyroclastic flows, which are commonly rich in accretionary lapilli.

The finer fraction of ejecta particles resided for a longer time in the flow and was more strongly affected by thermal alteration. This led to complete recrystallization of carbonate particles and to complete decomposition of euhedral calcite microcrystals in aggregates of calcite with silicate melt.

(4) For a period of presumably days to weeks (Artemieva and Morgan, 2009), the impactor component was deposited from suspension in the stratosphere, together with the finest fraction of both ejecta material—mainly ash-sized (partially fragmented) carbonate melt particles and temperature-resistant shocked quartz particles—and locally derived sediments. The presence of spherulitic carbonate melt spheroids in subunit 4 at El Guayal, which are also observed in the underlying ejecta units, together with shocked quartz and the PGE-enriched impactor component (Goderis et al., 2013), supports the theory that the Chicxulub impact triggered the mass extinction at the Cretaceous-Paleogene boundary (e.g., Schulte et al., 2010; Hull et al., 2020).

(5) The prolonged transport of impact debris in the hot ejecta plume and reaction with hot volatiles may have induced a particular style of alteration in the ejecta deposits. At El Guayal, silica was released during the alteration of silicate melt particles. This resulted in an intense silicification of recrystallized calcite particles and the microcrystalline calcite matrix in accretionary lapilli, and coherent precipitation of sparitic calcite in the interconnected pore space. These cementing processes may have enhanced the sealing properties of the ejecta deposits on top of the megabreccias that act as the oil-producing reservoir facies of the Cantarel oil fields in the Campeche marine platform (Grajales-Nishimura et al., 2000, 2009).

In summary, the presence of various aggregates at different Cretaceous-Paleogene sites indicates that aggregation processes potentially reduced the amount of particles and ash in the atmosphere, which possibly lowered the duration of global darkening. The abundant presence of calcium carbonate melts and recrystallized calcite at El Guayal and other Cretaceous-Paleogene sites collectively supports the conclusion that the amount of CO_2 released to the atmosphere during the Chicxulub impact has been probably overestimated (Agrinier et al., 2001; Ivanov and Deutsch, 2002; Skála et al., 2002). The rare presence of dolomite only in the lower ejecta subunits of El Guayal indicates that this mineral was strongly affected by dissociation. The exothermic back-reaction of CaO from decomposed carbonates and sulfates with CO_2 (and H_2O) to form $CaCO_3$ (Agrinier et al., 2001; Yancey and Guillemette, 2008) may have been responsible for a prolonged release of thermal energy ($\Delta H = -178$ kJ/mol) and delayed water vapor release during plume evolution.

ACKNOWLEDGMENTS

This study was partially supported by a Deutsche Forschungsgemeinschaft (DFG) Research Training Group (GRK 503) scholarship to T. Salge. We thank Philippe Claeys for providing samples, initial support, and guidance; Kirsten Born, Peter Czaja, Irmgard Felber, Hwa Ja Götz, Hans-Rudolf Knöfler, and Elke Wäsch for laboratory assistance; Dieter Stöffler for support; and Peter Schulte and Chiara Maria Petrone for their helpful comments and suggestions. Alessandro Montanari and an anonymous reviewer provided insightful, constructive reviews.

REFERENCES CITED

Addison, W.D., Brumpton, G.R., Vallini, D.A., McNaughton, N.J., Davis, D.W., Kissin, S.A., Fralick, P.W., and Hammond, A.L., 2005, Discovery of distal ejecta from the 1850 Ma Sudbury impact event: Geology, v. 33, p. 193–196, https://doi.org/10.1130/G21048.1.

Agrinier, P., Deutsch, A., Schärer, U., and Martínez, I., 2001, Fast back-reactions of shock released CO_2 from carbonates: An experimental approach: Geochimica et Cosmochimica Acta, v. 65, p. 2615–2632, https://doi.org/10.1016/S0016-7037(01)00617-2.

Alegret, L., Arenillas, I., Arz, J.A., Diaz, C., Grajales-Nishimura, J.M., Melendez, A., Molina, E., Rojas, R., and Soria, A.R., 2005, Cretaceous-Paleogene boundary deposits at Loma Capiro, central Cuba: Evidence for the Chicxulub impact: Geology, v. 33, p. 721–724, https://doi.org/10.1130/G21573.1.

Alvarez, L.W., Alvarez, W., Asaro, F., and Michel, H.V., 1980, Extraterrestrial cause for the Cretaceous-Tertiary extinction: Science, v. 208, p. 1095–1108, https://doi.org/10.1126/science.208.4448.1095.

Alvarez, W., Smit, J., Lowrie, W., Asaro, F., Margolis, S.V., Claeys, P., Kastner, M., and Hildebrand, A.R., 1992, Proximal impact deposits at the Cretaceous-Tertiary boundary in the Gulf of Mexico: A restudy of DSDP leg 77 Sites 536 and 540: Geology, v. 20, p. 697–700, https://doi.org/10.1130/0091-7613(1992)020<0697:PIDATC>2.3.CO;2.

Alvarez, W., Claeys, P., and Kieffer, S.W., 1995, Emplacement of KT boundary shocked quartz from Chicxulub crater: Science, v. 269, p. 930–935, https://doi.org/10.1126/science.269.5226.930.

Ames, D.E., Kjarsgaard, I.M., Pope, K.O., Dressler, B., and Pilkington, M., 2004, Secondary alteration of the impactite and mineralization in the basal Tertiary sequence, Yaxcopoil-1, Chicxulub impact crater, Mexico: Meteoritics & Planetary Science, v. 39, p. 1145–1167, https://doi.org/10.1111/j.1945-5100.2004.tb01134.x.

Arenillas, I., Arz, J.A., Grajales-Nishimura, J.M., Murillo-Muneton, G., Alvarez, W., Camargo-Zanoguera, A., Molina, E., and Rosales-Dominguez, C., 2006, Chicxulub impact event is Cretaceous/Paleogene boundary in age: New micropaleontological evidence: Earth and Planetary Science Letters, v. 249, p. 241–257, https://doi.org/10.1016/j.epsl.2006.07.020.

Artemieva, N., and Morgan, J., 2009, Modeling the formation of the K-Pg boundary layer: Icarus, v. 201, p. 768–780, https://doi.org/10.1016/j.icarus.2009.01.021.

Artemieva, N.A., Wünnemann, K., Krien, F., Reimold, W.U., and Stöffler, D., 2013, Ries crater and suevite revisited—Observations and modeling: Part

II. Modeling: Meteoritics & Planetary Science, v. 48, p. 590–627, https://doi.org/10.1111/maps.12085.

Artemieva, N., Morgan, J., and Expedition 364 Science Party, 2017, Quantifying the release of climate-active gases by large meteorite impacts with a case study of Chicxulub: Geophysical Research Letters, v. 44, p. 10180–10188, https://doi.org/10.1002/2017GL074879.

Bell, M.S., 2016, CO_2 release due to impact devolatilization of carbonate: Results of shock experiments: Meteoritics & Planetary Science, v. 51, p. 619–646, https://doi.org/10.1111/maps.12613.

Belza, J., Goderis, S., Montanari, A., Vanhaecke, F., and Claeys, P., 2017, Petrography and geochemistry of distal spherules from the K-Pg boundary in the Umbria-Marche region (Italy) and their origin as fractional condensates and melts in the Chicxulub impact plume: Geochimica et Cosmochimica Acta, v. 202, p. 231–263, https://doi.org/10.1016/j.gca.2016.12.018.

Beruto, D.T., Searcy, A.W., and Kim, M.G., 2004, Microstructure, kinetic, structure, thermodynamic analysis for calcite decomposition: Free-surface and powder bed experiments: Thermochimica Acta, v. 424, p. 99–109, https://doi.org/10.1016/j.tca.2004.05.027.

Bohor, B.F., Triplehorn, D.M., Nichols, D.J., and Millard, H.T., Jr., 1987, Dinosaurs, spherules, and the "magic" layer: A new K-T boundary clay site in Wyoming: Geology, v. 15, p. 896–899, https://doi.org/10.1130/0091-7613(1987)15<896:DSATML>2.0.CO;2.

Boslough, M.B., Ahrens, T.J., Vizgirda, J., Becker, R.H., and Epstein, S., 1982, Shock-induced devolatilization of calcite: Earth and Planetary Science Letters, v. 61, p. 166–170, https://doi.org/10.1016/0012-821X(82)90049-8.

Bralower, T.J., Paull, C.K., and Leckie, R.M., 1998, The Cretaceous-Tertiary boundary cocktail: Chicxulub impact triggers margin collapse and extensive sediment gravity flows: Geology, v. 26, p. 331–334, https://doi.org/10.1130/0091-7613(1998)026<0331:TCTBCC>2.3.CO;2.

Bralower, T.J., Cosmidis, J., Heaney, P.J., Kump, L.R., Morgan, J.V., Harper, D.T.,.Lyons, S.L., Freeman, K.H., Grice, K., Wendler, J.E., Zachos, J.C., Artemieva, N., Chen, S.A., Gulick, S.P.S., House, C.H., Jones, H.L., Lowery, C.M., Nims, C., Schaefer, B., Thomas, E., and Vajda V., 2020, Origin of a global carbonate layer deposited in the aftermath of the Cretaceous-Paleogene boundary impact: Earth and Planetary Science Letters, v. 548, 116476, https://doi.org/10.1016/j.epsl.2020.116476.

Branney, M.J., and Brown, R.J., 2011, Impactoclastic density current emplacement of terrestrial meteorite-impact ejecta and the formation of dust pellets and accretionary lapilli: Evidence from Stac Fada, Scotland: The Journal of Geology, v. 119, p. 275–292, https://doi.org/10.1086/659147.

Brown, R.J., Branney, M.J., Maher, C., and Davila-Harris, P., 2010, Origin of accretionary lapilli within ground-hugging density currents: Evidence from pyroclastic couplets on Tenerife: Geological Society of America Bulletin, v. 122, p. 305–320, https://doi.org/10.1130/B26449.1.

Brugger, J., Feulner, G., and Petri, S., 2017, Baby, it's cold outside: Climate model simulations of the effects of the asteroid impact at the end of the Cretaceous: Geophysical Research Letters, v. 44, p. 419–427, https://doi.org/10.1002/2016GL072241.

Burns, E., Sigurdsson, H., Carey, S., and D'Hondt, S., 2003, Geochemistry of accretionary lapilli from a Cretaceous-Tertiary impact breccia, Guayal, Mexico: Abstract 4132 presented at Third International Conference on Large Meteorite Impacts, Nördlingen, Germany, 5–7 August.

Claeys, P., Kiessling, W., and Alvarez, W., 2002, Distribution of Chicxulub ejecta at the Cretaceous-Tertiary boundary, *in* Koeberl, C., and MacLeod, K.G., eds., Catastrophic Events and Mass Extinctions: Impacts and Beyond: Geological Society of America Special Paper 356, p. 55–68, https://doi.org/10.1130/0-8137-2356-6.55.

Claeys, P., Heuschkel, S., Lounejeva-Baturina, E., Sanchez-Rubio, G., and Stöffler, D., 2003, The suevite of the drill hole Yucatán 6 in the Chicxulub impact structure: Meteoritics & Planetary Science, v. 38, p. 1299–1317, https://doi.org/10.1111/j.1945-5100.2003.tb00315.x.

Couture, R.A., 1985a, Rapid increase in permeability and porosity of bentonite-sand mixtures due to alteration by water vapor: Materials Research Society Symposium Proceedings, v. 44, p. 515–522.

Couture, R.A., 1985b, Steam rapidly reduces the swelling capacity of bentonite: Nature, v. 318, p. 50–52, https://doi.org/10.1038/318050a0.

Davis, J., 1973, Statistics and Data Analysis in Geology: New York, John Wiley & Sons, 550 p.

Dressler, B.O., Sharpton, V.L., Schwandt, C.S., and Ames, D., 2004, Impactites of the Yaxcopoil-1 drilling site, Chicxulub impact structure: Petrography, geochemistry, and depositional environment: Meteoritics & Planetary Science, v. 39, p. 857–878, https://doi.org/10.1111/j.1945-5100.2004.tb00935.x.

Dubron, L., Grajales-Nishimura, J.M., Alvarez, W., and Claeys, P., 2006, Breccia and fall-out suevite in the El Guayal KT section (Tabasco, Mexico): Geological Society of America Abstracts with Programs, v. 38, no. 7, p. 297.

Engelhardt, W.v., Andt, J., Fecker, B., and Pankau, H.G., 1995, Suevite breccia from the Ries crater, Germany: Origin, cooling history and devitrification of impact glasses: Meteoritics, v. 30, p. 279–293, https://doi.org/10.1111/j.1945-5100.1995.tb01126.x.

Fecker, B., 1993, Kristallisationsexperimente an natürlichen Suevitgläsern und Modellrechnungen zur Abkühlungsgeschichte des Fall-out Suevits im Nördlinger Ries [Ph.D. thesis]: Berlin, Germany, Freie Universität Berlin, 760 p.

Fisher, R.V., and Schmincke, H.-U., 1984, Pyroclastic Rocks: Berlin, Springer, 472 p., https://doi.org/10.1007/978-3-642-74864-6.

Fouke, B.W., Zerkle, A.L., Alvarez, W., Pope, K.O., Ocampo, A.C., Wachtman, R.J., Grajales Nishimura, J.M., Claeys, P., and Fischer, A.G., 2002, Cathodoluminescence petrography and isotope geochemistry of KT impact ejecta deposited 360 km from the Chicxulub crater, at Albion Island, Belize: Sedimentology, v. 49, p. 117–138, https://doi.org/10.1046/j.1365-3091.2002.00435.x.

French, B.M., 1998, Traces of Catastrophe: A Handbook of Shock-Metamorphic Effects in Terrestrial Meteorite Impact Structures: Houston, Texas, Lunar and Planetary Institute Contribution 954, 120 p.

Geisler, T., Janssen, A., Scheiter, D., Stephan, T., Berndt, J., and Putnis, A., 2010, Aqueous corrosion of borosilicate glass under acidic conditions: A new corrosion mechanism: Journal of Non-Crystalline Solids, v. 356, p. 1458–1465, https://doi.org/10.1016/j.jnoncrysol.2010.04.033.

Gilbert, J.S., and Lane, S.J., 1994, The origin of accretionary lapilli: Bulletin of Volcanology, v. 56, p. 398–411, https://doi.org/10.1007/BF00326465.

Goderis, S., Tagle, R., Belza, J., Smit, J., Montanari, A., Vanhaecke, F., Erzinger, J., and Claeys, P., 2013, Reevaluation of siderophile element abundances and ratios across the Cretaceous-Paleogene (K-Pg) boundary: Implications for the nature of the projectile: Geochimica et Cosmochimica Acta, v. 120, p. 417–446, https://doi.org/10.1016/j.gca.2013.06.010.

Grajales-Nishimura, J.M., Esteban, C.-P., Rosales-Domínguez, C., Morán-Zenteno, D.J., Alvarez, W., Claeys, P., Ruíz-Morales, J., García-Hernández, J., Padilla-Avila, P., and Sánchez-Ríos, A., 2000, Chicxulub impact: The origin of reservoir and seal facies in the southeastern Mexico oil fields: Geology, v. 28, p. 307–310, https://doi.org/10.1130/0091-7613(2000)28<307:CITOOR>2.0.CO;2.

Grajales-Nishimura, J.M., Murillo-Muñetón, G., Rosales-Domínguez, C., Bermúdez-Santana, J.C., Velasquillo, L., García-Hernández, J., Arz, J.A., and Arenillas, I., 2009, The Cretaceous-Paleogene boundary Chicxulub impact: Its effect on carbonate sedimentation on the western margin of the Yucatan platform and nearby areas, *in* Bartolini, C., and Román-Ramos, J.R., eds., Petroleum Systems in the southern Gulf of Mexico: American Association of Petroleum Geologists Memoir 90, p. 315– 335, https://doi.org/10.1306/13191090M902954.

Graup, G., 1981, Terrestrial chondrules, glass spherules and accretionary lapilli from the suevite, Ries crater, Germany: Earth and Planetary Science Letters, v. 55, p. 407–418, https://doi.org/10.1016/0012-821X(81)90168-0.

Graup, G., 1999, Carbonate-silicate liquid immiscibility upon impact melting: Ries crater, Germany: Meteoritics & Planetary Science, v. 34, p. 425–438, https://doi.org/10.1111/j.1945-5100.1999.tb01351.x.

Grieve, R.A.F., Ames, D.E., Morgan, J.V., and Artemieva, N., 2010, The evolution of the Onaping Formation at the Sudbury impact structure: Meteoritics & Planetary Science, v. 45, p. 759–782, https://doi.org/10.1111/j.1945-5100.2010.01057.x.

Griscom, D.L., Beltrán-López, V., Merzbacher, C.I., and Bolden, E., 1999, Electron spin resonance of 65-million-year-old glasses and rocks from the Cretaceous-Tertiary boundary: Journal of Non-Crystalline Solids, v. 253, p. 1–22, https://doi.org/10.1016/S0022-3093(99)00340-3.

Griscom, D., Beltrán-López, V., Pope, K.O., and Ocampo, A.C., 2003, New geochemical insights from electron-spin-resonance studies of Mn^{2+} and SO^{3-} in calcites: Quantitative analyses of Chicxulub crater ejecta from Belize and southern Mexico with comparison to limestones from distal Cretaceous-Tertiary boundary sites, *in* Koeberl, C., and Martínez-Ruiz, F., eds., Impact Markers in the Stratigraphic Record: Impact Studies: Berlin, Springer, p. 229–270, https://doi.org/10.1007/978-3-642-55463-6_10.

Gulick, S., Morgan, J., Mellett, C.L., Green, S.L., Bralower, T., Chenot, E., Christeson, G., Claeys, P., Cockell, C., Coolen, M.J.L, Ferrière, L., Gebhardt, C., Goto, K., Jones, H., Kring, D., Lofi, J., Lowery, C., Ocampo-Torres, R., Perez-Cruz, L., Pickersgill, A.E., Poelchau, M., Rae, A., Rasmussen, C., Rebolledo-Vieyra, M., Riller, U., Sato, H., Smit, J., Tikoo, S., Tomioka, N., Urrutia-Fucugauchi, J., Whalen, M., Wittmann, A., Yamaguchi, K., Xiao, L., and Zylberman, W., 2017a, Site M0077: Upper peak ring, *in* Morgan, J., Gulick, S., et al., eds., Chicxulub: Drilling the K-Pg Impact Crater: Proceedings of the International Ocean Discovery Program, Volume 364: College Station, Texas, Ocean Drilling Program, https://doi.org/10.14379/iodp.proc.364.106.2017.

Gulick, S., Morgan, J., Mellett, C.L., Green, S.L., Bralower, T., Chenot, E., Christeson, G., Claeys, P., Cockell, C., Coolen, M.J.L, Ferrière, L., Gebhardt, C., Goto, K., Jones, H., Kring, D., Lofi, J., Lowery, C., Ocampo-Torres, R., Perez-Cruz, L., Pickersgill, A.E., Poelchau, M., Rae, A., Rasmussen, C., Rebolledo-Vieyra, M., Riller, U., Sato, H., Smit, J., Tikoo, S., Tomioka, N., Urrutia-Fucugauchi, J., Whalen, M., Wittmann, A., Yamaguchi, K., Xiao, L., and Zylberman, W., 2017b, Site M0077: Post-impact sedimentary rocks, *in* Morgan, J., Gulick, S., Mellett, C.L., Green, S.L., and the Expedition 364 Scientists, eds., Chicxulub: Drilling the K-Pg Impact Crater: Proceedings of the International Ocean Discovery Program, Volume 364: College Station, Texas, Ocean Drilling Program, https://doi.org/10.14379/iodp.proc.364.105.2017.

Hamann, C., Bläsing, S., Hecht, L., Schäffer, S., Deutsch, A., Osterholz, J., and Lexow, B., 2018, The reaction of carbonates in contact with laser-generated, superheated silicate melts: Constraining impact metamorphism of carbonate-bearing target rocks: Meteoritics & Planetary Science, v. 53, p. 1644–1686, https://doi.org/10.1111/maps.13133.

Harvey, M.C., Brassell, S.C., Belcher, C.M., and Montanari, A., 2008, Combustion of fossil organic matter at the Cretaceous-Paleogene (K-P) boundary: Geology, v. 36, p. 355–358, https://doi.org/10.1130/G24646A.1.

Hecht, L., Wittmann, A., Schmitt, R.T., and Stöffler, D., 2004, Composition of impact melt particles and the effects of post-impact alteration in suevitic rocks at the Yaxcopoil-1 drill core, Chicxulub crater, Mexico: Meteoritics & Planetary Science, v. 39, p. 1169–1186, https://doi.org/10.1111/j.1945-5100.2004.tb01135.x.

Heuschkel, S., Lounejeva Baturina, E., Jones, A.P., Sanchez-Rubio, G., Claeys, P., and Stöffler, D., 1998, Carbonate melt in the suevite breccia of the Chicxulub crater [abs.]: Eos (Washington, D.C.), v. 79, p. F554.

Hildebrand, A.R., Penfield, G.T., Kring, D.A., Pilkington, M., Camargo, Z.A., Jacobsen, S.B., and Boynton, W.V., 1991, Chicxulub crater: A possible Cretaceous/Tertiary boundary impact crater on the Yucatán Peninsula, Mexico: Geology, v. 19, p. 867–871, https://doi.org/10.1130/0091-7613(1991)019<0867:CCAPCT>2.3.CO;2.

Hörz, F., Archer, P.D., Niles, P.B., Zolensky, M.E., and Evans, M., 2015, Devolatilization or melting of carbonates at Meteor Crater, AZ?: Meteoritics & Planetary Science, v. 50, p. 1050–1070, https://doi.org/10.1111/maps.12453.

Hörz, F., Cintala, M.J., Thomas-Keprta, K.L., Ross, D.K., and Clemett, S.J., 2020, Unconfined shock experiments: A pilot study into the shock-induced melting and devolatilization of calcite: Meteoritics & Planetary Science, v. 55, p. 102–129, https://doi.org/10.1111/maps.13424.

Huber, M.S., and Koeberl, C., 2017, Accretionary lapilli from the Sudbury impact event: Meteoritics & Planetary Science, v. 52, p. 1257–1276, https://doi.org/10.1111/maps.12863.

Hull, P.M., Bornemann, A., Penman, D.E., Henehan, M.J., Norris, R.D., Wilson, P.A., Blum, P., Alegret, L., Batenburg, S.J., Bown, P.R., Bralower, T.J., Cournede, C., Deutsch, A., Donner, B., Friedrich, O., Jehle, S., Kim, H., Kroon, D., Lippert, P.C., Loroch, D., Moebius, I., Moriya, K., Peppe, D.J., Ravizza, G.E., Röhl, U., Schueth, J.D., Sepúlveda, J., Sexton, P.F., Sibert, E.C., Śliwińska, K.K., Summons, R.E., Thomas, E., Westerhold, T., Whiteside, J.H., Yamaguchi, T., and Zachos, J.C., 2020, On impact and volcanism across the Cretaceous-Paleogene boundary: Science, v. 367, p. 266–272, https://doi.org/10.1126/science.aay5055.

Ivanov, B.A., and Deutsch, A., 2002, The phase diagram of $CaCO_3$ in relation to shock compression and decomposition: Physics of the Earth and Planetary Interiors, v. 129, p. 131–143, https://doi.org/10.1016/S0031-9201(01)00268-0.

Ivanov, B.A., Badukov, D.D., Yakovlev, O.I., Gerasimov, M.V., Dikov, Y.P., Pope, K.O., and Ocampo, A.C., 1996, Degassing of sedimentary rocks due to the Chicxulub impact: Hydrocode and physical simulations, *in* Ryder, G., Fastovsky, D., and Gartner, S., eds., The Cretaceous-Tertiary Boundary Event and Other Catastrophes in Earth History: Geological Society of America Special Paper 307, p. 125−140, https://doi.org/10.1130/0-8137-2307-8.125.

Izett, G.A., 1990, The Cretaceous/Tertiary Boundary Interval, Raton Basin, Colorado and New Mexico, and Its Content of Shock-Metamorphosed Minerals: Evidence Relevant to the K/T Boundary Impact-Extinction Event: Geological Society of America Special Paper 249, 100 p., https://doi.org/10.1130/SPE249-p1.

James, M.R., Gilbert, J.S., and Lane, S.J., 2002, Experimental investigation of volcanic particle aggregation in the absence of a liquid phase: Journal of Geophysical Research–Solid Earth, v. 107, 2191, https://doi.org/10.1029/2001jb000950.

Japan Nuclear Cycle Development Institute (JNC), 2000, H12: Project to Establish Technical Basis for HLW Disposal in Japan: Supporting Report 2. Repository Design and Engineering Technology: Tokai, Japan Nuclear Cycle Development Institute, JNC TN1410 2000–003, 711 p.

Jarosewich, E., Gooley, R., and Husler, J., 1987, Chromium augite—A new microprobe reference sample: Geostandards Newsletter, v. 11, p. 197–198, https://doi.org/10.1111/j.1751-908X.1987.tb00027.x.

Jarosewich, E., Nelen, J.A., and Norberg, J.A., 1980, Reference samples for electron microprobe analysis: Geostandards Newsletter, v. 4, p. 43–47, https://doi.org/10.1111/j.1751-908X.1980.tb00273.x.

Johnson, B.C., and Melosh, H.J., 2014, Formation of melt droplets, melt fragments, and accretionary impact lapilli during a hypervelocity impact: Icarus, v. 228, p. 347–363, https://doi.org/10.1016/j.icarus.2013.10.022.

Jones, A.P., Claeys, P., and Heuschkel, S., 2000, Impact melting of carbonates from the Chicxulub impact crater, *in* Gilmour, I., and Koeberl, C., eds., Impacts and the Early Earth: Lecture Notes in Earth Sciences: Berlin, Springer, p. 343–361, https://doi.org/10.1007/BFb0027767.

Kenkmann, T., and Schönian, F., 2006, Ries and Chicxulub: Impact craters on Earth provide insights for Martian ejecta blankets: Meteoritics & Planetary Science, v. 41, p. 1587–1603, https://doi.org/10.1111/j.1945-5100.2006.tb00437.x.

Kieffer, S.W., and Simonds, C.H., 1980, The role of volatiles and lithology in the impact cratering process: Reviews of Geophysics and Space Physics, v. 18, p. 143–181, https://doi.org/10.1029/RG018i001p00143.

King, D.T., and Petruny, L.W., 2003, Stratigraphy and sedimentology of coarse impactoclastic breccia units within the Cretaceous-Tertiary boundary section, Albion Island, Belize, *in* Koeberl, C., and Martínez-Ruiz, F., eds., Impact Markers in the Stratigraphic Record: Impact Studies: Berlin, Springer, p. 203–227, https://doi.org/10.1007/978-3-642-55463-6_9.

King, D.T., and Petruny, L.W., 2015, Correlation of northern Belize's Cretaceous-Paleogene ('KT') boundary sections: Gulf Coast Association of Geological Societies Transactions, v. 65, p. 463–473.

Kletetschka, G., Ocampo Uria, A., Zila, V., and Elbra, T., 2020, Electric discharge evidence found in a new class of material in the Chicxulub ejecta: Scientific Reports, v. 10, 9035, https://doi.org/10.1038/s41598-020-65974-2.

Koeberl, C., Brandstätter, F., Glass, B.P., Hecht, L., Mader, D., and Reimold, W.U., 2007, Uppermost impact fallback layer in the Bosumtwi crater (Ghana): Mineralogy, geochemistry, and comparison with Ivory Coast tektites: Meteoritics & Planetary Science, v. 42, p. 709–729, https://doi.org/10.1111/j.1945-5100.2007.tb01069.x.

Kring, D.A., and Durda, D.D., 2002, Trajectories and distribution of material ejected from the Chicxulub impact crater: Implications for postimpact wildfires: Journal of Geophysical Research–Planets, v. 107, p. 6-1–6-22, https://doi.org/10.1029/2001je001532.

Kring, D.A., Hörz, F., Zürcher, L., and Urrutia-Fucugauchi, J., 2004, Impact lithologies and their emplacement in the Chicxulub impact crater: Initial results from the Chicxulub Scientific Drilling Project, Yaxcopoil, Mexico: Meteoritics & Planetary Science, v. 39, p. 879–897, https://doi.org/10.1111/j.1945-5100.2004.tb00936.x.

Krogh, T.E., Kamo, S.L., Sharpton, V.L., Marin, L.E., and Hildebrand, A.R., 1993, U-Pb ages of single shocked zircons linking distal K/T ejecta to the Chicxulub crater: Nature, v. 366, p. 731–734, https://doi.org/10.1038/366731a0.

Kruge, M.A., Stankiewicz, B.A., Crelling, J.C., Montanari, A., and Bensley, D.F., 1994, Fossil charcoal in Cretaceous-Tertiary boundary strata: Evidence for catastrophic firestorm and megawave: Geochimica et Cosmochimica Acta, v. 58, p. 1393–1397, https://doi.org/10.1016/0016-7037(94)90394-8.

Langenhorst, F., and Deutsch, A., 2012, Shock metamorphism of minerals: Elements, v. 8, p. 31–36, https://doi.org/10.2113/gselements.8.1.31.

Le Maitre, R.W., 1979, A new generalised petrological mixing system: Contributions to Mineralogy and Petrology, v. 71, p. 133–137, https://doi.org/10.1007/BF00375429.

Lopez-Ramos, E., 1975, Geological summary of the Yucatán Peninsula, *in* Nairn, A.E.M., and Stehli, F.G., eds., Ocean Basins and Margins: The Gulf of Mexico and the Caribbean: New York, Plenum Press, p. 257–282, https://doi.org/10.1007/978-1-4684-8535-6_7.

Machel, H.G., Mason, R.A., Mariano, A.N., and Mucci, A., 1991, Causes and emission of luminescence in calcite and dolomite, *in* Barker, C.A., and Kopp, O.C., eds., Luminescence Microscopy and Spectroscopy—Qualitative and Quantitative Applications: Tulsa, Oklahoma, Society for Sedimentary Geology (SEPM), Book 25 p. 9–25, https://doi.org/10.2110/scn.91.25.0009.

MacLeod, K.G., Whitney, D.L., Huber, B.T., and Koeberl, C., 2007, Impact and extinction in remarkably complete Cretaceous-Tertiary boundary sections from Demerara Rise, tropical western North Atlantic: Geological Society of America Bulletin, v. 119, p. 101–115, https://doi.org/10.1130/B25955.1.

Melosh, H.J., 1989, Impact Cratering: A Geologic Process: New York, Oxford University Press, Oxford Monographs on Geology and Geophysics 11, 245 p.

Melosh, J., 2001, Deep down at Chicxulub: Nature, v. 414, p. 861–862, https://doi.org/10.1038/414861a.

Meyer, C., 2012, Sedimentological, Structural and Geochemical Investigations of the Suevite of the Impact Crater Nördlinger Ries, Germany [Ph.D. thesis]: Berlin, Germany, Freie Universität Berlin, 130 p.

Montanari, A., 1991, Authigenesis of impact spheroids in the K/T boundary clay from Italy; new constraints for high-resolution stratigraphy of terminal Cretaceous events: Journal of Sedimentary Research, v. 61, p. 315–339, https://doi.org/10.1306/D42676FE-2B26-11D7-8648000102C1865D.

Montanari, A., Hay, R.L., Alvarez, W., Asaro, F., Michel, H.V., Alvarez, L.W., and Smit, J., 1983, Spheroids at the Cretaceous-Tertiary boundary are altered impact droplets of basaltic composition: Geology, v. 11, p. 668–671, https://doi.org/10.1130/0091-7613(1983)11<668:SATCBA>2.0.CO;2.

Moore, J.G., and Peck, D.L., 1962, Accretionary lapilli in volcanic rocks of the western continental United States: The Journal of Geology, v. 70, p. 182–193, https://doi.org/10.1086/626807.

Morgan, J., Warner, M., the Chicxulub Working Group, Brittan, J., Buffler, R., Camargo, A., Christeson, G., Denton, P., Hildebrand, A., Hobbs, R., Macintyre, H., Mackenzie, G., Maguire, P., Marin, L., Nakamura, Y., Pilkington, M., Sharpton, V., Snyder, D., Suarez, G., and Trejo, A., 1997, Size and morphology of the Chicxulub impact crater: Nature, v. 390, p. 472–476, https://doi.org/10.1038/37291.

Morgan, J.V., Gulick, S.P., Bralower, T., Chenot, E., Christeson, G., Claeys, P., Cockell, C., Collins, G.S., Coolen, M.J.L., Ferrière, L., Gebhardt, C., Goto, K., Jones, H., Kring, D.A., Le Ber, E., Lofi, J., Long, X., Lowery, C., Mellett, C., Ocampo-Torres, R., Osinski, G.R., Perez-Cruz, L., Pickersgill, A., Poelchau, M., Rae, A., Rasmussen, C., Rebolledo-Vieyra, M., Riller, U., Sato, H., Schmitt, D.R., Smit, J., Tikoo, S., Tomioka, N., Urrutia-Fucugauchi, J., Whalen, M., Wittmann, A., Yamaguchi, K.E., and Zylberman, W., 2016, The formation of peak rings in large impact craters: Science, v. 354, p. 878–882, https://doi.org/10.1126/science.aah6561.

Moropoulou, A., Bakolas, A., and Aggelakopoulou, E., 2001, The effects of limestone characteristics and calcination temperature to the reactivity of the quicklime: Cement and Concrete Research, v. 31, p. 633–639, https://doi.org/10.1016/S0008-8846(00)00490-7.

Mueller, S.B., Kueppers, U., Huber, M.S., Hess, K.U., Poesges, G., Ruthensteiner, B., and Dingwell, D.B., 2018, Aggregation in particle rich environments: A textural study of examples from volcanic eruptions, meteorite impacts, and fluidized bed processing: Bulletin of Volcanology, v. 80, p. 32, https://doi.org/10.1007/s00445-018-1207-3.

Muir, T.L., and Peredery, W.V., 1984, The Onaping Formation, *in* Pye, E.G., Naldrett, A.J., and Giblin, P.E., eds., The Geology and Ore Deposits of the Sudbury Structure: Ontario Geological Survey Special Volume 1, p. 139–210.

Nelson, M.J., Newsom, H.E., Spilde, M.N., and Salge, T., 2012, Petrographic investigation of melt and matrix relationships in Chicxulub crater Yaxcopoil-1 brecciated melt rock and melt rock–bearing suevite (846–885 m, units 4 and 5): Geochimica et Cosmochimica Acta, v. 86, p. 1–20, https://doi.org/10.1016/j.gca.2012.02.022.

Neuser, R.D., Bruhn, F., Götze, J., Habermann, D., and Richter, D.K., 1996, Kathodenlumineszenz: Methodik und Anwendung: Zentralblatt Geologie und Paläontologie, v. 1 (1995 1/2), p. 287–306.

Norris, R.D., Huber, B.T., and Self-Trail, J., 1999, Synchroneity of the K-T oceanic mass extinction and meteorite impact: Blake Nose, western North Atlantic: Geology, v. 27, p. 419–422, https://doi.org/10.1130/0091-7613(1999)027<0419:SOTKTO>2.3.CO;2.

Ocampo, A.C., Pope, K.O., and Fisher, A.G., 1996, Ejecta blanket deposits of the Chicxulub crater from Albion island, Belize, *in* Ryder, G., Fastovsky, D., and Gartner, S., eds., The Cretaceous-Tertiary Boundary Event and Other Catastrophes in Earth History: Geological Society of America Special Paper 307, p. 75–88, https://doi.org/10.1130/0-8137-2307-8.75.

Ocampo, A.C., Pope, K.O., and Fischer, A.G., 1997a, Carbonate ejecta from the Chicxulub crater: Evidence for ablation and particle interactions under high temperatures and pressures, *in* Lunar and Planetary Science Conference XXVIII: Houston, Texas, Lunar Planetary Institute, abstract 1861, CD-ROM.

Ocampo, A., Pope, K., Marshall, J., and Fischer, A., 1997b, Surface textures produced by grain interaction under high temperature: Comparison of Chicxulub ejecta and laboratory experiments: Geological Society of America Abstracts with Programs, v. 29, p. 142.

O'Keefe, J.D., and Ahrens, T.J., 1989, Impact production of CO_2 by the Cretaceous/Tertiary extinction bolide and the resultant heating of the Earth: Nature, v. 338, p. 247–249, https://doi.org/10.1038/338247a0.

Osinski, G.R., and Spray, J.G., 2001, Impact-generated carbonate melts: Evidence from the Haughton structure, Canada: Earth and Planetary Science Letters, v. 194, p. 17–29, https://doi.org/10.1016/S0012-821X(01)00558-1.

Osinski, G.R., Spray, J.G., and Grieve, R.A.F., 2008, Impact melting in sedimentary target rocks: An assessment, *in* Evans, K.R., Horton, J.W., Jr., King, D.T., Jr., and Morrow, J.R., eds., The Sedimentary Record of Meteorite Impacts: Geological Society of America Special Paper 437, p. 1–17, https://doi.org/10.1130/2008.2437(01).

Osinski, G.R., Grieve, R.A.F., Hill, P.J.A., Simpson, S.L., Cockell, C., Christeson, G.L., Ebert, M., Gulick, S., Melosh, H.J., Riller, U., Tikoo, S.M., and Wittmann, A., 2019, Explosive interaction of impact melt and seawater following the Chicxulub impact event: Geology, v. 48, p. 108–112, https://doi.org/10.1130/G46783.1.

Peucker-Ehrenbrink, B., and Jahn, B.M., 2001, Rhenium-osmium isotope systematics and platinum group element concentrations: Loess and the upper continental crust: Geochemistry Geophysics Geosystems, v. 2, https://doi.org/10.1029/2001GC000172.

Pierazzo, E., and Artemieva, N., 2012, Local and global environmental effects of impact on Earth: Elements, v. 8, p. 55–60, https://doi.org/10.2113/gselements.8.1.55.

Pierazzo, E., Kring, D.A., and Melosh, H.J., 1998, Hydrocode simulation of the Chicxulub impact event and the production of climatically active gases: Journal of Geophysical Research–Planets, v. 103, p. 28,607–28,625, https://doi.org/10.1029/98JE02496.

Pollastro, R.M., and Bohor, B.F., 1993, Origin and clay-mineral genesis of the Cretaceous/Tertiary boundary unit, Western Interior of North America: Clays and Clay Minerals, v. 41, p. 7–25, https://doi.org/10.1346/CCMN.1993.0410102.

Pope, K.O., Baines, H.K., Ocampo, A.C., and Ivanov, B., 1997, Energy, volatile production, and climate effects of the Chicxulub Cretaceous/Tertiary boundary impact: Journal of Geophysical Research, v. 102, p. 21,645–21,664, https://doi.org/10.1029/97JE01743.

Pope, K.O., Ocampo, A.C., Fisher, A.G., Alvarez, W., Fouke, B.W., Webster, C.L., Vega, F.J., Smit, J., Fritsche, A.E., and Claeys, P., 1999, Chicxulub impact ejecta from Albion Island, Belize: Earth and Planetary Science Letters, v. 170, p. 351–364, https://doi.org/10.1016/S0012-821X(99)00123-5.

Pope, K.O., Ocampo, A.C., Fischer, A.G., Vega, F.J., Ames, D.E., King, D.T., Fouke, B.W., Wachtmann, R.J., and Kletetschka, G., 2005, Chicxulub impact ejecta in southern Quintana Roo, México and central Belize, *in* Kenkmann, T., Hörz, F., and Deutsch, A., eds., Large Meteorite Impacts III: Geological Society of America Special Paper 384, p. 171–190, https://doi.org/10.1130/0-8137-2384-1.171.

Pusch, R., 2000, On the Effect of Hot Water Vapor on MX-80 Clay: Stockholm, Sweden, Swedish Nuclear Fuel and Waste Management Co. (SKB) Technical Report 00–16, 41 p.

Pusch, R., and Karnland, O., 1988, Geological Evidence of Smectite Longevity. The Sardinian and Gotland Cases: Stockholm, Sweden, Swedish Nuclear Fuel and Waste Management Co. (SKB) Technical Report 88-26, 60 p.

Pusch, R., Karnland, O., Hökmark, H., Sandén, T., and Börgesson, L., 1991, Final Report of the Rock Sealing Project—Sealing Properties and Longevity of Smectitic Clay Grouts: Stockholm, Sweden, Swedish Nuclear Fuel and Waste Management Co. (SKB), Stripa Project Technical Report 91-30, 36 p.

Pusch, R., Karnland, O., Lajudie, A., Lechelle, J., and Bouchet, A., 1993, Hydrothermal Field Test with French Candidate Clay Embedding Steel Heater in the Stripa Mine: Stockholm, Sweden, Swedish Nuclear Fuel and Waste Management Co. (SKB) Technical Report 93-02, 85 p.

Renne, P.R., Deino, A.L., Hilgen, F.J., Kuiper, K.F., Mark, D.F., Mitchell, W.S., III, Morgan, L.E., Mundil, R., and Smit, J., 2013, Time scales of critical events around the Cretaceous-Paleogene boundary: Science, v. 339, p. 684–687, https://doi.org/10.1126/science.1230492.

Riley, T.R., and Leat, P.T., 1999, Large volume silicic volcanism along the proto-Pacific margin of Gondwana: Lithological and stratigraphical investigations from the Antarctic Peninsula: Geological Magazine, v. 136, p. 1–16, https://doi.org/10.1017/S0016756899002265.

Rose, W.I., Delene, D.J., Schneider, D.J., Bluth, G.J.S., Krueger, A.J., Sprod, I., Mckee, C., Davies, H.L., and Ernst, G.G.J., 1995, Ice in the 1994 Rabaul eruption cloud—Implications for volcano hazard and atmospheric effects: Nature, v. 375, p. 477–479, https://doi.org/10.1038/375477a0.

Salge, T., Stosnach, H., Rosatelli, G., Hecht, L., and Reimold, W.U., 2019, Evidence for shock-induced anhydrite recrystallization and decomposition at the UNAM-7 drill core from the Chicxulub impact structure: Meteoritics & Planetary Science, v. 54, p. 2334–2356, https://doi.org/10.1111/maps.13283.

Schmitt, R.T., Wittmann, A., and Stoffler, D., 2004, Geochemistry of drill core samples from Yaxcopoil-1, Chicxulub impact crater, Mexico: Meteoritics & Planetary Science, v. 39, p. 979–1001, https://doi.org/10.1111/j.1945-5100.2004.tb00940.x.

Schulte, P., and Kontny, A., 2005, Chicxulub impact ejecta from the Cretaceous-Paleogene (K-P) boundary in northeastern México, *in* Kenkmann, T., Hörz, F., and Deutsch, A., eds., Large Meteorite Impacts III: Geological Society of America Special Paper 384, p. 191–221, https://doi.org/10.1130/0-8137-2384-1.191.

Schulte, P., Stinnesbeck, W., Stüben, D., Kramar, U., Berner, Z., Keller, G., and Adatte, T., 2003, Fe-rich and K-rich mafic spherules from slumped and channelized Chicxulub ejecta deposits in the northern La Sierrita area, NE Mexico: International Journal of Earth Sciences, v. 92, p. 114–142, https://doi.org/10.1007/s00531-002-0304-9.

Schulte, P., Speijer, R.P., Mai, H., and Kontny, A., 2006, The Cretaceous-Paleogene (K-P) boundary at Brazos, Texas: Sequence stratigraphy, depositional events and the Chicxulub impact: Sedimentary Geology, v. 184, p. 77–109, https://doi.org/10.1016/j.sedgeo.2005.09.021.

Schulte, P., Deutsch, A., Salge, T., Berndt, J., Kontny, A., MacLeod, K.G., Neuser, R.D., and Krumm, S., 2009, A dual-layer Chicxulub ejecta sequence with shocked carbonates from the Cretaceous-Paleogene (K-Pg) boundary, Demerara Rise, western Atlantic: Geochimica et Cosmochimica Acta, v. 73, p. 1180–1204, https://doi.org/10.1016/j.gca.2008.11.011.

Schulte, P., Alegret, L., Arenillas, I., Arz, J.A., Barton, P.J., Bown, P.R., Bralower, T.J., Christeson, G.L., Claeys, P., Cockell, C.S., Collins, G.S., Deutsch, A., Goldin, T.M., Goto, K., Grajales-Nishimura, J.M., Grieve, R.A.F., Gulick, S.P.S., Johnson, K.R., Kiessling, W., Koeberl, C., Kring, D.A., MacLeod, K.G., Matsui, T., Melosh, J., Montanari, A., Morgan, J.V., Neal, C.R., Nichols, D.J., Norris, R.D., Pierazzo, E., Ravizza, G., Rebolledo-Vieyra, M., Reimold, W.U., Robin, E., Salge, T., Speijer, R.P. Sweet, A.R., Urrutia-Fucugauchi, J., Vajda, V., Whalen, M.T., and Willumsen, P.S., 2010, The Chicxulub asteroid impact and mass extinction at the Cretaceous-Paleogene boundary: Science, v. 327, p. 1214–1218, https://doi.org/10.1126/science.1177265.

Schulte, P., Smit, J., Deutsch, A., Salge, T., Friese, A., and Beichel, K., 2012, Tsunami backwash deposits with Chicxulub impact ejecta and dinosaur remains from the Cretaceous-Palaeogene boundary in the La Popa Basin, Mexico: Sedimentology, v. 59, p. 737–765, https://doi.org/10.1111/j.1365-3091.2011.01274.x.

Schumacher, R., and Schmincke, H.U., 1995, Models for the origin of accretionary lapilli: Bulletin of Volcanology, v. 56, p. 626–639, https://doi.org/10.1007/BF00301467.

Sharpton, V.L., Burke, K., Camargo-Zanoguera, A., Hall, S.A., Lee, D.S., Marin, L.E., Suárez-Reynoso, G., Quezada-Muneton, J.M., Spudis, P.D., and Urrutia-Fucugauchi, J., 1993, Chicxulub multiring impact basin: Size and other characteristics derived from gravity analysis: Science, v. 261, p. 1564–1567, https://doi.org/10.1126/science.261.5128.1564.

Sharpton, V.L., Corrigan, C.M., Marin, L.E., Urrutia-Fucugauchi, J., and Vogel, T.A., 1999, Characterization of impact breccias from the Chicxulub impact basin: Implications for excavation and ejecta emplacement, *in* Lunar and Planetary Science Conference XXX: Houston, Texas, Lunar and Planetary Institute, abstract 1515, CD-ROM.

Sigurdsson, H., D'Hondt, S., and Carey, S., 1995, Geochemistry of the Cretaceous/Tertiary impact ejecta deposit in Mexico and Belize, *in* Lunar and Planetary Science Conference XXII: Houston, Texas, Lunar and Planetary Institute, abstract 1301–1302.

Skála, R., Ederová, J., Matjka, P., and Hörz, F., 2002, Mineralogical investigations of experimentally shocked dolomite: Implications for the outgassing of carbonates, *in* Koeberl, C., and MacLeod, K.G., eds., Catastrophic Events and Mass Extinctions: Geological Society of America Special Paper 356, p. 571–585, https://doi.org/10.1130/0-8137-2356-6.571.

Smit, J., 1999, The global stratigraphy of the Cretaceous-Tertiary boundary impact ejecta: Annual Review of Earth and Planetary Sciences, v. 27, p. 75–113, https://doi.org/10.1146/annurev.earth.27.1.75.

Smit, J., Alvarez, W., Montanari, A., Swinburne, N., van Kempen, T.M., Klaver, G.T., and Lustenhouwer, W.J., 1992, "Tektites" and microkrystites at the Cretaceous Tertiary boundary: Two strewn fields, one crater?, *in* Proceedings of Lunar and Planetary Science Conference XXII: Houston, Texas, Lunar and Planetary Institute, p. 87–100.

Smit, J., Roep, T.B., Alvarez, W., Montanari, A., Claeys, P., Grajales Nishimura, J.M., and Bermudez, J., 1996, Coarse-grained, clastic sandstone complex at the KT boundary around the Gulf of Mexico: Deposition by tsunami waves induced by the Chicxulub impact, *in* Ryder, G., Fastovsky, D., and Gartner, S., eds., The Cretaceous-Tertiary Boundary Event and Other Catastrophes in Earth History: Geological Society of America Special Paper 307, p. 151–182, https://doi.org/10.1130/0-8137-2307-8.151.

Stöffler, D., 1971, Progressive metamorphism and classification of shocked and brecciated crystalline rocks at impact craters: Journal of Geophysical Research, v. 76, p. 5541–5551, https://doi.org/10.1029/JB076i023p05541.

Stöffler, D., Artemieva, N.A., Ivanov, B.A., Hecht, L., Kenkmann, T., Schmitt, R.T., Tagle, R.A., and Wittmann, A., 2004, Origin and emplacement of the impact formations at Chicxulub, Mexico, as revealed by the ICDP deep drilling at Yaxcopoil-1 and by numerical modeling: Meteoritics & Planetary Science, v. 39, p. 1035–1067, https://doi.org/10.1111/j.1945-5100.2004.tb01128.x.

Stöffler, D., Artemieva, N.A., Wünnemann, K., Reimold, W.U., Jacob, J., Hansen, B.K., and Summerson, I.A.T., 2013, Ries crater and suevite revisited—Observations and modeling: Part I. Observations: Meteoritics & Planetary Science, v. 48, p. 515–589, https://doi.org/10.1111/maps.12086.

Swisher, C.C., III, Grajales-Nishimura, J.M., Montanari, A., Margolis, S.V., Claeys, P., Alvarez, W., Renne, P., Cedillo-Pardoa, E., Maurrasse, F.J.-M.R., Curtis, G.H., Smit, J., and McWilliams, M.O., 1992, Coeval $^{40}Ar/^{39}Ar$ ages of 65.0 million years ago from Chicxulub crater melt rock and Cretaceous-Tertiary boundary tektites: Science, v. 257, p. 954–958, https://doi.org/10.1126/science.257.5072.954.

Tabor, C.R., Bardeen, C.G., Otto-Bliesner, B.L., Garcia, R.R., and Toon, O.B., 2020, Causes and climatic consequences of the impact winter at the Cretaceous-Paleogene boundary: Geophysical Research Letters, v. 47, e60121, https://doi.org/10.1029/2019GL085572.

Tagle, R., and Berlin, J., 2008, A database of chondrite analyses including platinum group elements, Ni, Co, Au, and Cr: Implications for the identification of chondritic projectiles: Meteoritics & Planetary Science, v. 43, p. 541–559, https://doi.org/10.1111/j.1945-5100.2008.tb00671.x.

Tagle, R., Erzinger, J., Hecht, L., Schmitt, R.T., Stöffler, D., and Claeys, P., 2004, Platinum group elements in impactites of the ICDP Chicxulub drill core Yaxcopoil-1: Are there traces of the projectile?: Meteoritics & Planetary Science, v. 39, p. 1009–1016, https://doi.org/10.1111/j.1945-5100.2004.tb00942.x.

Telling, J., and Dufek, J., 2012, An experimental evaluation of ash aggregation in explosive volcanic eruptions: Journal of Volcanology and Geothermal Research, v. 209–210, p. 1–8, https://doi.org/10.1016/j.jvolgeores.2011.09.008.

Tuchscherer, M.G., Reimold, W.U., Koeberl, C., Gibson, R.L., and Bruin, D.D., 2004a, First petrographic results on impactites from the Yaxcopoil-1 borehole, Chicxulub structure, Mexico: Meteoritics & Planetary Science, v. 39, p. 899–930, https://doi.org/10.1111/j.1945-5100.2004.tb00937.x.

Tuchscherer, M.G., Reimold, W.U., Koeberl, C., and Gibson, R.L., 2004b, Major and trace element characteristics of impactites from the Yaxcopoil-1 borehole, Chicxulub structure, Mexico: Meteoritics & Planetary Science, v. 39, p. 955–978, https://doi.org/10.1111/j.1945-5100.2004.tb00939.x.

Tuchscherer, M.G., Reimold, W.U., Koeberl, C., and Gibson, R.L., 2005, Geochemical and petrographic characteristics of impactites and Cretaceous target rocks from the Yaxcopoil-1 borehole, Chicxulub impact structure, Mexico: Implications for target compositions: Meteoritics & Planetary Science, v. 40, p. 1513–1536, https://doi.org/10.1111/j.1945-5100.2005.tb00415.x.

Urrutia-Fucugauchi, J., Marín, L., and Trejo-García, A., 1996, Initial results of the UNAM scientific drilling program on the Chicxulub impact structure: Rock magnetic properties of UNAM-7 Tekax borehole: Geofísica Internacional, v. 35, p. 125–133.

Urrutia-Fucugauchi, J., Pérez-Cruz, L., Campos-Arriola, S.E., Escobar-Sánchez, E., and Velasco-Villarreal, M., 2014, Magnetic susceptibility logging of Chicxulub proximal impact breccias in the Santa Elena borehole: Implications for emplacement mode: Studia Geophysica et Geodaetica, v. 58, p. 100–120, https://doi.org/10.1007/s11200-013-0803-0.

Vellekoop, J., Esmeray-Senlet, S., Miller, K.G., Browning, J.V., Sluijs, A., van de Schootbrugge, B., Sinninghe Damsté, J.S., and Brinkhuis, H., 2016, Evidence for Cretaceous-Paleogene boundary bolide "impact winter" conditions from New Jersey, USA: Geology, v. 44, p. 619–622, https://doi.org/10.1130/G37961.1.

Wali, A., 1985, Abkühlung der Suevite im Nördlinger Ries [Diploma thesis]: Tübingen, Germany, University of Tübingen, 65 p.

Walton, E.L., Timms, N.E., Hauck, T.E., MacLagan, E.A., and Herd, C.D.K., 2019, Evidence of impact melting and post-impact decomposition of sedimentary target rocks from the Steen River impact structure, Alberta, Canada: Earth and Planetary Science Letters, v. 515, p. 173–186, https://doi.org/10.1016/j.epsl.2019.03.015.

Warme, J.E., Morgan, M., and Kuehner, H.-C., 2002, Impact-generated carbonate accretionary lapilli in the Late Devonian Alamo Breccia, *in* Koeberl, C., and MacLeod, K.G., eds., Catastrophic Events and Mass Extinctions: Impacts and Beyond: Geological Society of America Special Paper 356, p. 489–504, https://doi.org/10.1130/0-8137-2356-6.489.

Wedepohl, K.H., 1995, The composition of the continental crust: Geochimica et Cosmochimica Acta, v. 59, p. 1217–1232, https://doi.org/10.1016/0016-7037(95)00038-2.

Wendler, J., and Willems, H., 2002, Distribution pattern of calcareous dinoflagellate cysts across the Cretaceous-Tertiary boundary (Fish Clay, Stevns Klint, Denmark): Implications for our understanding of species-selective extinction, *in* Koeberl, C., and MacLeod, K.G., eds., Catastrophic Events and Mass Extinctions: Impacts and Beyond: Geological Society of America Special Paper 356, p. 265–275, https://doi.org/10.1130/0-8137-2356-6.265.

Wittmann, A., Kenkmann, T., Schmitt, R.T., Hecht, L., and Stöffler, D., 2004, Impact-related dike breccia lithologies in the ICDP drill core Yaxcopoil-1, Chicxulub impact structure, Mexico: Meteoritics & Planetary Science, v. 39, p. 931–954, https://doi.org/10.1111/j.1945-5100.2004.tb00938.x.

Yancey, T.E., and Guillemette, R.N., 2008, Carbonate accretionary lapilli in distal deposits of the Chicxulub impact event: Geological Society of America Bulletin, v. 120, p. 1105–1118, https://doi.org/10.1130/B26146.1.

Zürcher, L., and Kring, D.A., 2004, Hydrothermal alteration in the core of the Yaxcopoil-1 borehole, Chicxulub impact structure, Mexico: Meteoritics & Planetary Science, v. 39, p. 1199–1221, https://doi.org/10.1111/j.1945-5100.2004.tb01137.x.

Manuscript Accepted by the Society 20 November 2020
Manuscript Published Online 9 June 2021